IOPscience iopscience.iop.org

Home Search Collections Journals About Contact us My IOPscience

Interplay between electron–phonon and Coulomb interactions in cuprates

This article has been downloaded from IOPscience. Please scroll down to see the full text article.

2008 J. Phys.: Condens. Matter 20 043201

(http://iopscience.iop.org/0953-8984/20/4/043201)

View the table of contents for this issue, or go to the journal homepage for more

Download details:
IP Address: 129.252.86.83
The article was downloaded on 29/05/2010 at 08:03

Please note that terms and conditions apply.

IOP PUBLISHING JOURNAL OF PHYSICS: CONDENSED MATTER

J. Phys.: Condens. Matter **20** (2008) 043201 (22pp) doi:10.1088/0953-8984/20/04/043201

TOPICAL REVIEW

Interplay between electron–phonon and Coulomb interactions in cuprates

O Gunnarsson[1] **and O Rösch**[1,2]

[1] Max-Planck-Institut für Festkörperforschung, D-70506 Stuttgart, Germany
[2] Institut für Theoretische Physik, Universität zu Köln, D-50937 Köln, Germany

Received 30 August 2007, in final form 8 November 2007
Published 8 January 2008
Online at stacks.iop.org/JPhysCM/20/043201

Abstract
Evidence for strong electron–phonon coupling in high-T_c cuprates is reviewed, with emphasis on the electron and phonon spectral functions. Effects due to the interplay between the Coulomb and electron–phonon interactions are studied. For weakly doped cuprates, the phonon self-energy is strongly reduced due to correlation effects, while there is no corresponding strong reduction for the electron self-energy. Polaron formation is studied, focusing on effects of Coulomb interaction and antiferromagnetic correlations. It is argued that experimental indications of polaron formation in undoped cuprates are due to a strong electron–phonon interaction for these systems.

(Some figures in this article are in colour only in the electronic version)

Contents

1. Introduction

High-T_c cuprates show a large number of interesting features, apart from the exceptionally large superconducting transition temperature T_c. They exhibit antiferromagnetic [1], pseudogap [2], marginal Fermi liquid [3] and ordinary Fermi liquid phases in addition to the superconducting phase. After the high-T_c cuprates had been discovered [4], there was initially much interest in the electron–phonon interaction (EPI). It was, however, soon concluded that the EPI is too weak to explain superconductivity alone, in particular d-wave superconductivity, and the interest focused on purely electronic

 © 2008 IOP Publishing Ltd Printed in the UK

models of these compounds. More recently, there has been substantial experimental evidence that the EPI plays an appreciable role for a number of properties. Certain phonons show a large softening and broadening under doping [5, 6], suggesting a strong interaction with doped holes. This is, for instance, seen for the so-called half-breathing copper–oxygen bond-stretching phonon, apical oxygen phonons and the oxygen B_{1g} buckling phonon. Photoemission spectroscopy (PES) experiments show the formation of small polarons for the undoped cuprates [7], and a kink in the nodal **k**-direction also suggests strong EPI [8]. While there is only a weak isotope effect on T_c for optimally doped samples, a strong isotope effect has been seen away from optimum doping [9]. Recent STM work suggests that a phonon mode plays a role in superconductivity [10], although other interpretations are possible [11]. In particular, an isotope effect has been observed [10]. While the phonon contribution to superconductivity remains unclear, it seems clear that phonons can be important for other properties.

The EPI has been studied very extensively in the local density approximation (LDA) [12] of the density functional formalism [13], which is particularly appropriate for systems where correlation effects are not very strong. This approach has been shown to be very successful for conventional superconductors [14–17]. For cuprates [18] a rather weak EPI was found, which alone would not be sufficient to explain the superconductivity [19]. However, the calculated width [20] of the half-breathing phonon is an order of magnitude smaller than the reported experimental value [21], raising questions about the accuracy of the LDA in this context [22]. An even larger width and softening has been observed for an apical oxygen phonon [5]. The coupling to this mode is mainly electrostatic and probably too efficiently screened in the LDA [23]. The interest has therefore recently focused on whether the interplay between the Coulomb interaction and the EPI can explain experimental signs of a strong EPI.

Due to the important effects of the Coulomb interaction in these systems, models such as the Hubbard and t–J models are often used. In these models important phonons couple to charge fluctuations. Since charge fluctuations are strongly suppressed in the cuprates by the Coulomb interaction, an important issue is whether this could mean that the EPI is actually suppressed. We discuss this issue extensively below.

In the so-called sudden approximation, angular resolved photoemission spectroscopy (ARPES) can be directly related to the one-electron Green's function. If superconductivity is due to bosons coupling to electrons and forming electron pairs, this coupling should show up in the one-electron Green's function. Due to the high energy resolution and **k**-resolution that can now be obtained in ARPES, a lot of interest has focused on ARPES recently, and we address these issues below.

ARPES experiments strongly indicate that small polarons are formed for undoped cuprates and there are signs of strong phonon side bands [7]. This indicates that there is a strong EPI for these systems. For weakly underdoped or optimally doped cuprates, ARPES experiments show quasiparticles, suggesting that there are no small polarons formed in these cases [7]. However, there is still substantial spectral weight in the energy range where phonon side bands would be expected, suggesting that the EPI is still substantial. Optical experiments are also often interpreted in terms of polarons [24–29]. There has been extensive work on polarons and bipolarons, treating both electronic properties in general and superconductivity [24, 26, 28]. Since experiments suggest that small polarons are not formed at dopings relevant for superconductivity [7], we here focus on polaron formation for insulating systems.

Due to the great interest in cuprates, there have been many reviews covering different aspects of these systems [1, 2, 5, 6, 8, 9, 18, 30–34, 28, 35–41].

2. Models

2.1. Coulomb interaction and hopping

The Coulomb interaction plays an important role in the cuprates. A frequently used model for describing this is the three-band model [42], which includes a Cu $x^2 - y^2$ 3d orbital and two O orbitals in a CuO_2 plane. The model includes the Cu–O hopping integrals and the Coulomb interaction between two electrons on the Cu orbital.

$$H_{\text{three-band}} = \varepsilon_d \sum_{i\sigma} c^\dagger_{i\sigma} c_{i\sigma} + \varepsilon_O \sum_{i\delta\sigma} a^\dagger_{i\delta\sigma} a_{i\delta\sigma} + t_{pd} \sum_{i\delta\sigma} P_\delta (c^\dagger_{i\sigma} a_{i\delta\sigma} + \text{H.c.}) + U \sum_i n_{i\uparrow} n_{i\downarrow}, \quad (1)$$

where ε_d and ε_O are the energies of the Cu and O atoms, respectively. $\boldsymbol{\delta}$ describes the O atom positions in the unit cell and runs over $(a/2, 0)$ and $(0, a/2)$ in the second term and over $(\pm a/2, 0)$ and $(0, \pm a/2)$ in the third term, where a is the lattice parameter. $P_{-\boldsymbol{\delta}} = -P_{\boldsymbol{\delta}}$, $P_{\boldsymbol{\delta}} = 1$ for $\delta = (a/2, 0)$ and $P_{\boldsymbol{\delta}} = -1$ for $\delta = (0, a/2)$. $c^\dagger_{i\sigma}$ creates a Cu electron in cell i with spin σ, $a^\dagger_{i\boldsymbol{\delta}\sigma}$ creates an O electron and $n_\sigma = c^\dagger_{i\sigma} c_{i\sigma}$. U is the Coulomb interaction and t_{pd} is a hopping integral.

From this model the t–J model can be derived [43], where each site corresponds to a Cu atom in the CuO_2 plane. In the undoped system, corresponding to all Cu atoms being in d^9 configurations, each site is occupied by one hole. In a hole doped system, the holes go primarily onto the O sites. Such an O hole forms a Zhang–Rice singlet with a Cu hole [43]. A Zhang–Rice singlet is described by an empty site in the t–J model. The corresponding Hamiltonian is

$$H_{t-J} = -t \sum_{\langle ij\rangle\sigma} (\tilde{c}^\dagger_{i\sigma} \tilde{c}_{j\sigma} + \text{H.c.}) + J \sum_{\langle ij\rangle} (\mathbf{S}_i \cdot \mathbf{S}_j - \tfrac{1}{4} n_i n_j), \quad (2)$$

where $\langle ij\rangle$ refers to a sum over nearest neighbor pairs, and $\tilde{c}^\dagger_{i\sigma}$ creates a spin σ hole on-site i if this site was previously empty. $\mathbf{S}_i$ is the spin and $n_i = \sum_\sigma \tilde{c}^\dagger_{i\sigma} \tilde{c}_{i\sigma}$ is the number of holes on site i.

Alternatively, the one-band Hubbard model is often used:

$$H_{\text{Hub}} = -t \sum_{\langle ij\rangle\sigma} (c^\dagger_{i\sigma} c_{j\sigma} + \text{H.c.}) + U \sum_i n_{i\uparrow} n_{i\downarrow}. \quad (3)$$

The t–J model can also be derived from the Hubbard model in the large U limit if certain terms are neglected [44].

2.2. Electron–phonon interaction

We introduce the Hamiltonian for a set of phonons

$$H_{\rm ph} = \sum_{\mathbf{q}} \hbar\omega_{\mathbf{q}} b^{\dagger}_{\mathbf{q}} b_{\mathbf{q}}, \tag{4}$$

where $b_{\mathbf{q}}$ annihilates a phonon with the frequency $\omega_{\mathbf{q}}$ and the wavevector $\mathbf{q}$. Generally we write the coupling to the phonons as

$$H_{\rm el-ph} = \frac{1}{\sqrt{N}} \sum_{\mathbf{kq}} g(\mathbf{k}, \mathbf{q}) c^{\dagger}_{\mathbf{k}+\mathbf{q}\sigma} c_{\mathbf{k}\sigma} (b_{\mathbf{q}} + b^{\dagger}_{-\mathbf{q}}), \tag{5}$$

where N is the number of cells.

2.2.1. Holstein phonons. Often, the electron–phonon interaction is treated in a Holstein model, where there is an on-site coupling to one local Einstein phonon per site. This corresponds to a $\mathbf{k}$ and $\mathbf{q}$ independent coupling

$$g_{\rm Hol}(\mathbf{k}, \mathbf{q}) = g_0, \tag{6}$$

where g_0 is the coupling constant, and a $\mathbf{q}$ independent phonon frequency $\omega_{\mathbf{q},\rm Hol} = \omega_{\rm ph}$.

2.2.2. Breathing phonons. The breathing (oxygen bond-stretching) phonons have attracted much interest due to the observation of an anomalous softening and broadening of these phonons when the system is doped [5]. That these phonons may have a strong coupling can be understood by noticing that the formation of the Zhang–Rice singlet in the t–J model involves a large energy of the order of several eV. For a system without phonons and a fixed number of doped holes, this energy only enters as an uninteresting constant. If phonons are added, however, the singlet energy can be modulated by the phonons. This is the case for the breathing phonons, where the O atoms in the CuO_2 plane move in the direction of the Cu atoms, thereby changing the bond lengths (see figure 1). This directly modulates the Cu–O hopping integrals $t_{\rm pd}$ (in a three-band model) determining the Zhang–Rice singlet energy and leads to a substantial coupling. This has been discussed by several groups [45–51]. A general formula for this coupling was given in [51], considering both the modulation of the Cu–O hopping integrals and shifts of the levels due to Coulomb interactions. It was found that the main coupling is an on-site coupling due to the modulation of the Cu–O hopping integrals. One reason for this result is that the hopping integrals in the t–J model, obtained after the O levels have been projected out, are about an order of magnitude smaller than the on-site singlet energy. This strongly favors the on-site electron–phonon interaction over the coupling to the t–J hopping integrals[3]. Below we therefore neglect the off-site interaction. If we furthermore assume that the vibration of the Cu atom can be neglected due to its larger mass, the oxygen phonon eigenvectors can be approximated as $\epsilon^{\alpha}_{\alpha} = \sin(aq_{\alpha}/2)/\sqrt{\sin^2(aq_x/2) + \sin^2(aq_y/2)}$, where $\alpha = x$ or y,

[3] A substantial off-site coupling and therefore $\mathbf{k}$ dependence was found in [59], which, however, is due to an energy zero problem.

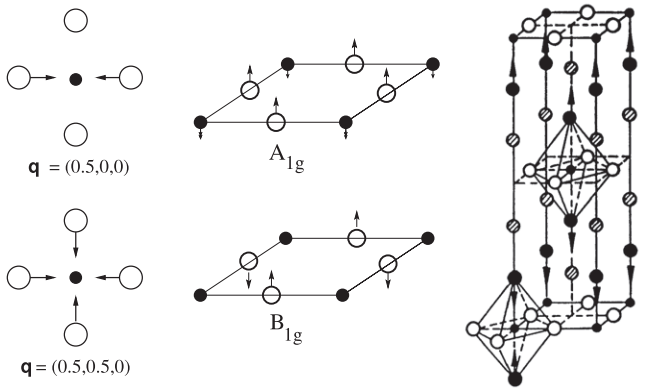

Figure 1. Half-breathing (upper left), breathing (lower left), A_{1g} (upper middle), B_{1g} (lower middle) and apical oxygen O^{Z}_{Z} (right) phonon modes. In the left and middle figures, the small filled circles show Cu atoms and the large circles O atoms in the CuO_2 plane. In the right figure (after Pintschovius and Reichardt [5]), the large black spheres show apical O atoms.

describing the motions in the directions of the nearest neighbor Cu atoms. Then the coupling becomes

$$g_{\rm Br}(\mathbf{k}, \mathbf{q}) \sim \sqrt{\sin^2(aq_{\alpha}/2) + \sin^2(aq_y/2)}, \tag{7}$$

i.e., the coupling depends on $\mathbf{q}$ but not on $\mathbf{k}$ in this approximation [52].

2.2.3. A_{1g} and B_{1g} phonons. There has been substantial interest in a B_{1g} phonon at about 42 meV [53–55], involving a motion perpendicular to the CuO_2 plane of the O atoms in this plane. These atoms can move out of phase, leading to a B_{1g} phonon, or in phase, leading to an A_{1g} phonon (see figure 1). Devereaux and co-workers [56–59] studied these phonons in the three-band model. They considered the case when there is an electrical field [60], E_z, perpendicular to the CuO_2 plane, due to different valencies of the ions on the two sides of a plane. Since the O atoms move perpendicular to the plane for the A_{1g} and B_{1g} phonons, these phonons couple to such a field. For the case of only nearest neighbor hopping, this leads to the coupling [59]

$$g_{A_{1g},B_{1g}}(\mathbf{k}, \mathbf{q}) \sim E_z[B_x \phi^{*}_{x}(\mathbf{k}+\mathbf{q})\phi_x(\mathbf{k}) + B_y \phi^{*}_{y}(\mathbf{k}+\mathbf{q})\phi_y(\mathbf{k})], \tag{8}$$

where $\phi^{x}_{y} = \mp i t^{x}_{y}(\mathbf{k})/\sqrt{E^2(\mathbf{k}) + \Omega^2(\mathbf{k})}$, $E(\mathbf{k}) = |\varepsilon_{\rm d} - \varepsilon_{\rm O}|/2 + \sqrt{(\varepsilon_{\rm d} - \varepsilon_{\rm O})^2/4 + \Omega^2(\mathbf{k})}$, $\Omega^2(\mathbf{k}) = t^2_x(\mathbf{k}) + t^2_y(\mathbf{k})$ and $t_{\alpha}(\mathbf{k}) = 2t\sin(ak_{\alpha}/2)$. Using a spring model, Devereaux *et al* [58] obtained the eigenvectors $[B_x, B_y] = [\cos(aq_y/2), -\cos(aq_x/2)]/M(\mathbf{q})$ for the B_{1g} mode, where $M(\mathbf{q}) = \sqrt{\cos^2(aq_y/2) + \cos^2(aq_x/2)}$. Putting the Cu mass equal to infinity, their model gives $[B_x, B_y] = [\cos(aq_x/2), \cos(aq_y/2)]/M(\mathbf{q})$ for the A_{1g} mode.

In contrast to the breathing phonons, these modes have a strong $\mathbf{k}$ dependence. For $\mathbf{q} = 0$, the coupling due to the B_{1g} phonon is entirely off site, while the A_{1g} phonon has a substantial on-site coupling.

A different approach was taken by Jepsen *et al* [61]. They studied a six-band model of the LDA band structure and

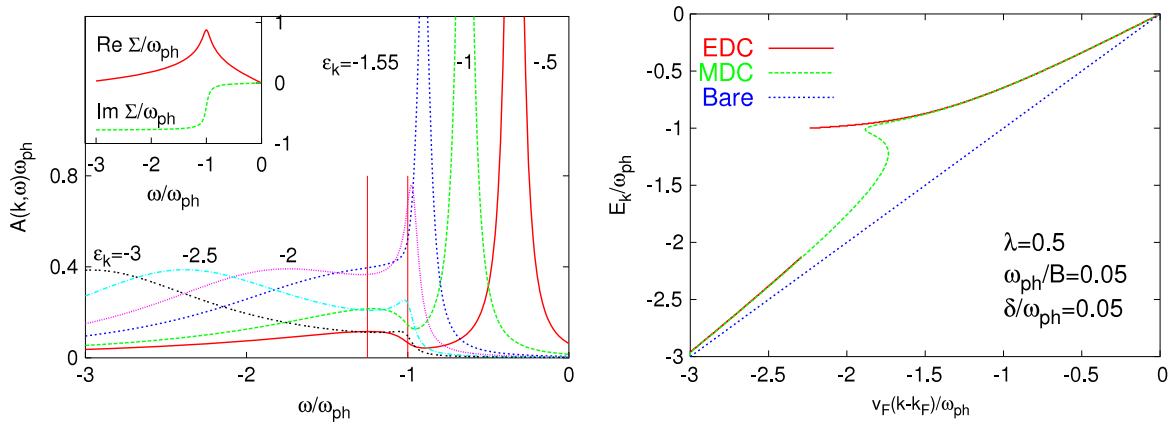

Figure 2. The spectral function (left), calculated for different values of the bare energy $\varepsilon_{\mathbf{k}}$ (in units of $\omega_{\rm ph}$), and the dispersion (right), comparing EDC and MDC results with the bare dispersion. The inset in the left part shows the real and imaginary part of Σ. All results are obtained for the model in equations (6), (11) and they have been given a Lorentzian broadening (FWHM) of 2δ. The parameters are $\lambda = 0.5$, $\omega_{\rm ph}/B = 0.05$ and $\delta/\omega_{\rm ph} = 0.05$.

focused on the coupling due to the modulation of hopping integrals. This coupling is zero for a completely flat CuO_2 plane but becomes finite for a dimpled plane. They obtained a coupling

$$g_{B_{1g}}(\mathbf{k},\mathbf{q}) \sim \cos\frac{a(k_x+q_x)}{2}\cos\frac{ak_x}{2} - \cos\frac{a(k_y+q_y)}{2}\cos\frac{ak_y}{2}. \tag{9}$$

This coupling tends to emphasize small values of $|\mathbf{k}|$ and $|\mathbf{k}+\mathbf{q}|$ more than equation (8), due to the appearance of cos functions rather than sin functions in $t_\alpha(\mathbf{k})$ entering equation (8).

2.2.4. Apical phonons. Neutron scattering experiments show that several apical oxygen phonons (see figure 1) broaden and soften when a cuprate is doped [5]. This coupling has been calculated for La_2CuO_4 using a shell model [23]. Due to the ionicity of the O atoms, the electrostatic part of the coupling is expected to be particularly strong. This is in particular true for the undoped system, which is an insulator, leading to a poor screening of the electrostatic interaction. It is therefore important not to perform this calculation using the LDA, since LDA gives a metallic system and too efficient screening. Due to the electrostatic nature of the coupling, and due to small $\mathbf{q}$ vectors playing an important role, the coupling is expected to be dominated by the on-site part of the coupling, i.e.,

$$g_{\rm Apical}(\mathbf{k},\mathbf{q}) \sim g_{\rm A}(\mathbf{q}). \tag{10}$$

Calculations showed that this coupling is indeed rather strong [23].

3. Weak coupling and noninteracting electrons

3.1. Electron self-energy

The electron–phonon interaction is often studied assuming that the electrons are noninteracting. This is a quite unrealistic assumption for the cuprates, where the electron–electron interaction is crucial. Below, we nevertheless describe some of the results [62–64] for this case, since they provide a basis for discussing similarities and deviations for strongly correlated systems. The electrons are described by the Hamiltonian

$$H_{\rm non} = \sum_{\mathbf{k}\sigma} \varepsilon_{\mathbf{k}} c^\dagger_{\mathbf{k}\sigma} c_{\mathbf{k}\sigma}, \tag{11}$$

where $\varepsilon_{\mathbf{k}}$ is the energy for the wavevector $\mathbf{k}$ and σ is a spin index. The electrons are assumed to couple to the phonons via the Holstein model (6). We calculate the retarded electron self-energy to lowest order in the coupling g. For $T = 0$, it is given by [62]

$$\Sigma(\mathbf{k},\omega) = \frac{1}{N} g^2 \sum_{\mathbf{q}} \left[\frac{f(\varepsilon_{\mathbf{k}+\mathbf{q}})}{\omega + \omega_{\rm ph} - \varepsilon_{\mathbf{k}+\mathbf{q}} + {\rm i}\delta} + \frac{1 - f(\varepsilon_{\mathbf{k}+\mathbf{q}})}{\omega - \omega_{\rm ph} - \varepsilon_{\mathbf{k}+\mathbf{q}} + {\rm i}\delta} \right], \tag{12}$$

where N is the number of sites, $f(\varepsilon)$ is the Fermi function and δ is a positive infinitesimal (later small) quantity. We assume that $N(\varepsilon) = 1/B$ is constant, where $N(\varepsilon)$ is the density of states (DOS) per spin and B is the band width. The band is assumed to be half-filled and to extend from $-B/2$ to $B/2$. Then the sum in equation (12) can be performed exactly, giving

$$\Sigma(\mathbf{k},\omega) = \frac{1}{2}\lambda\omega_{\rm ph}\left[\ln\frac{\omega + \omega_{\rm ph} + B/2 + {\rm i}\delta}{\omega + \omega_{\rm ph} + {\rm i}\delta} + \ln\frac{\omega - \omega_{\rm ph} + {\rm i}\delta}{\omega - \omega_{\rm ph} - B/2 + {\rm i}\delta} \right], \tag{13}$$

where

$$\lambda = \frac{2g^2}{\omega_{\rm ph}} N(0). \tag{14}$$

Σ is $\mathbf{k}$-independent in this approximation. Assuming that $\omega_{\rm ph} \ll B/2$, we obtain

$$\Sigma(\mathbf{k},\omega) = \begin{cases} -\lambda\omega, & \text{if } |\omega| \ll \omega_{\rm ph}; \\ 0, & \text{if } \omega_{\rm ph} \ll |\omega| \ll B/2. \end{cases} \tag{15}$$

Results for Σ are shown in the inset of figure 2. At $T = 0$, a hole with a binding energy larger than the phonon

frequency $\omega_{\rm ph}$ can excite a phonon and simultaneously be scattered. $|\,\mathrm{Im}\,\Sigma|$ is therefore large for $\omega < -\omega_{\rm ph}$. If the system is (s-wave) superconducting, scattering is only possible for binding energies larger than $\omega_{\rm ph} + \Delta$, where Δ is the gap, since the scattered electron has at least the binding energy Δ [64]. Related to the abrupt onset of Im Σ there is a logarithmic singularity in Re Σ. The left part of figure 2 shows the spectral function

$$A(\mathbf{k},\omega) = \frac{1}{\pi}\frac{|\mathrm{Im}\,\Sigma(\mathbf{k},\omega)|}{[\omega-\varepsilon_{\mathbf{k}}-\mathrm{Re}\Sigma(\mathbf{k},\omega)]^2+[\mathrm{Im}\,\Sigma(\mathbf{k},\omega)]^2}. \tag{16}$$

For simplicity, in figure 2 we have assumed a linear dispersion over the energy range of interest, $\varepsilon_{\mathbf{k}} = v_{\rm F}(k - k_{\rm F})$, where $v_{\rm F}$ and $k_{\rm F}$ are the Fermi velocity and wavevector, respectively. $A(\mathbf{k},\omega)$ shows a narrow peak at $E_{\mathbf{k}} = \varepsilon_{\mathbf{k}}/(1+\lambda)$ if $|E_{\mathbf{k}}| \ll \omega_{\rm ph}$ and it has a broad peak at $E_{\mathbf{k}} = \varepsilon_{\mathbf{k}}$ if $|\varepsilon_{\mathbf{k}}| \gg \omega_{\rm ph}$. The electron–phonon coupling therefore leads to a change of slope

$$\frac{|\mathrm{d}E_{\mathbf{k}}/\mathrm{d}\mathbf{k}|_{E_{\mathbf{k}}=0}}{|\mathrm{d}E_{\mathbf{k}}/\mathrm{d}\mathbf{k}|_{|E_{\mathbf{k}}|\gg\omega_{\rm ph}}} = \frac{1}{1+\lambda}. \tag{17}$$

We also define the quasiparticle strength

$$Z(\mathbf{k}) = \frac{1}{1-(\partial\Sigma(\mathbf{k},\omega)/\partial\omega)|_{\omega=E_{\mathbf{k}}}} = \frac{1}{1+\lambda}, \tag{18}$$

where the second equality is only valid for $|E_{\mathbf{k}}| \ll \omega_{\rm ph}$.

3.2. Energy and momentum distribution curves

Figure 2 shows energy distribution curves (EDCs), where $A(\mathbf{k},\omega)$ is shown as a function of ω for a fixed value of $\mathbf{k}$. For each value of $\mathbf{k}$ we can determine the ω for which $A(\mathbf{k},\omega)$ has its maximum. From this we obtain a dispersion relation $E_{\mathbf{k}}$ shown by the solid (red) curve (EDC) in the right part of the figure. From the results for $A(\mathbf{k},\omega)$ it is clear that the EDC dispersion jumps from $E_{\mathbf{k}}/\omega_{\rm ph} \approx -1$ for $\varepsilon_{\mathbf{k}}/\omega_{\rm ph} \approx -2$ to $E_{\mathbf{k}}/\omega_{\rm ph} \approx -2.1$ for $\varepsilon_{\mathbf{k}}/\omega_{\rm ph} \approx -2.3$. The EDC dispersion is reduced by a factor $(1+\lambda)$ close to $E_{\mathbf{k}} = 0$, as discussed below equation (16), and the dispersion is further reduced as $E_{\mathbf{k}}$ approaches $-\omega_{\rm ph}$.

Alternatively, we can study momentum distribution curves (MDCs), showing $A(\mathbf{k},\omega)$ as a function of $\mathbf{k}$ for a fixed ω. In particular, we can find the $\mathbf{k}$ for which $A(\mathbf{k},\omega)$ has its maximum (ω fixed). This MDC dispersion relation is shown in the right part of figure 2. As an illustration, the vertical lines in the left part of the figure show the energies $\omega/\omega_{\rm ph} = -1$ and -1.25. The maximum (among the $\mathbf{k}$ values shown in figure 2) of $A(\mathbf{k},\omega/\omega_{\rm ph} = -1)$ is obtained for $\varepsilon_{\mathbf{k}}/\omega_{\rm ph} = -2$, while the maximum of $A(\mathbf{k},\omega/\omega_{\rm ph} = -1.25)$ is obtained for $\varepsilon_{\mathbf{k}}/\omega_{\rm ph} = -1.55$. Over a certain frequency range, an *increase* in $|\omega|$ then leads to a *decrease* in $|\varepsilon_{\mathbf{k}}|$. The result is the S-like shape of the MDC dispersion around $\omega/\omega_{\rm ph} = -1$. Well away from this energy, the EDC and MDC curves agree for this $\mathbf{k}$-independent self-energy.

$A(\mathbf{k},\omega)$ tends to show a dip at $\omega \approx -\omega_{\rm ph}$, in particular if $0 > \varepsilon_{\mathbf{k}} > -\omega_{\rm ph}$ [64]. This is the combined effect of a logarithmic singularity in Re $\Sigma(\mathbf{k},\omega)$ at $\omega = -\omega_{\rm ph}$, which makes the first term in the denominator in equation (16) large, and the sudden onset of Im $\Sigma(\mathbf{k},\omega)$ below $\omega = -\omega_{\rm ph}$, which makes the numerator large. As discussed above, the singularity is shifted to $\omega_{\rm ph} + \Delta$ in a (s-wave) superconductor. At the same time the effect becomes stronger, since weight is piled up at the onset of Im $\Sigma(\mathbf{k},\omega)$, leading to a more pronounced structure in Re $\Sigma(\mathbf{k},\omega)$. As discussed by Sandvik *et al* [65], this effect is particularly pronounced for an s-wave superconductor and less strong for a d-wave superconductor.

Similarly, the phonon self-energy $\Pi(\mathbf{q},\omega)$ can be calculated to lowest order in g, where $\mathbf{q}$ is the phonon wavevector. Im $\Pi(\mathbf{q},\omega)$ is of particular interest, since it determines the phonon width. For a system of noninteracting electrons and a nondegenerate phonon mode, Allen [66, 67] showed that

$$2\,\mathrm{Im}\,\Pi(\omega_{\rm ph}) = 2\pi\hbar^2\omega_{\rm ph}^2 N(0)\lambda, \tag{19}$$

where $2\,\mathrm{Im}\,\Pi(\mathbf{q},\omega_{\rm ph})$ is the full width at half maximum (FWHM) and $N(0)$ is the density of states (DOS) per spin at the Fermi energy. Knowledge of the FWHM of the phonons then gives a possibility of estimating λ.

3.3. Electron–phonon coupling in the 2D Holstein model

Two-dimensional (2D) correlated models with EPI are often compared with the 2D Holstein model to determine the effects of correlation on the EPI. A 2D Holstein model at half-filling with only nearest neighbor hopping is unstable to an infinitesimal EPI due to perfect nesting. Therefore, the comparison is often made to a Holstein model with just a single electron at the bottom of the band [68, 69]. Often a t–J model doped with one hole is studied, suggesting similarities with a Holstein model with a single electron. The half-filled Holstein model, however, is of particular interest, since the relevant antibonding Cu–O band in the cuprates is close to half-filling.

3.3.1. Weak coupling limit. We consider the limit $g \ll t$ and $\omega_{\rm ph} \ll t$ for a nearest neighbor hopping t with a single electron Holstein model. Using the self-energy in equation (12), we can define an effective electron–phonon coupling $\lambda = \lambda_0$ via the quasiparticle weight Z (equation (18)) or the effective mass

$$\left.\frac{\mathrm{d}^2E_{\mathbf{k}}/\mathrm{d}\mathbf{k}^2}{\mathrm{d}^2\varepsilon_{\mathbf{k}}/\mathrm{d}\mathbf{k}^2}\right|_{\mathbf{k}=0} = \frac{1}{1+\lambda_0}, \tag{20}$$

where

$$\lambda_0 = \frac{g^2}{4\pi t\omega_{\rm ph}}. \tag{21}$$

Both methods give the same λ for this model in the weak coupling limit [70]. Instead of the Holstein model with a single electron, we can study the half-filled model assuming a constant density of states (DOS) and calculating $\Sigma(\mathbf{k},\omega)$ according to equation (13). Defining λ via the expression for $Z(\mathbf{k})$ recovers the λ defined in equation (14) and leads to $\lambda = \pi\lambda_0$, since $N(0) = 1/(8t)$. The increase in λ is partly due to the fact that the self-energy at the bottom of the band only has contributions from higher states while in the half-filled case there are contributions from both higher and lower states and partly due to the DOS at the bottom of the band being smaller than the average DOS [71].

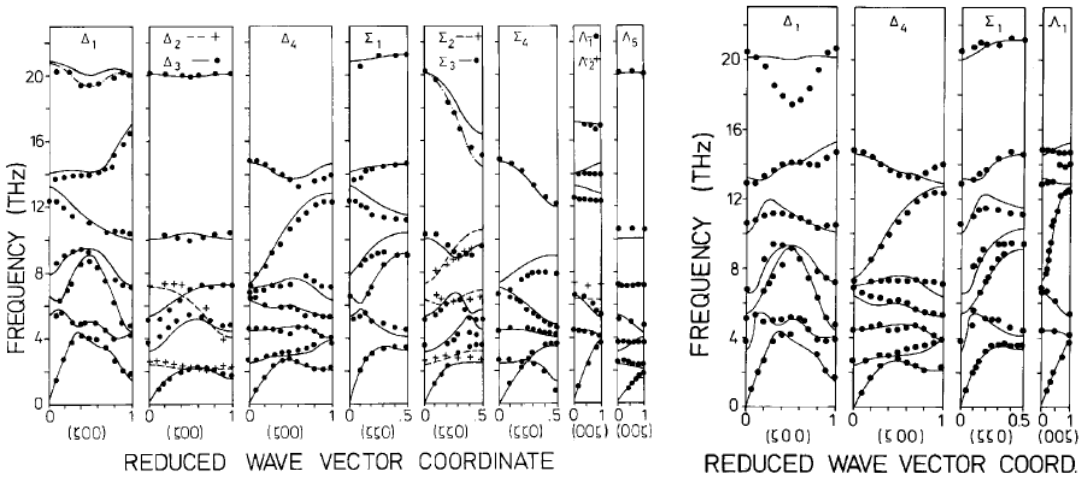

Figure 3. Phonon dispersion curves for La_2CuO_4 (left-hand side) and $La_{1.9}Sr_{0.1}CuO_4$ (right-hand side). The solid curves were calculated in a shell model by Chaplot *et al* [81]. The dash–dotted lines were obtained after inclusion of a quadrupolar force constant. The figure illustrates that in the doped compound (right-hand side) the half-breathing mode in the Δ_1 symmetry at 20 THz and several apical oxygen modes in the Λ_1 symmetry at 12–16 THz are softened (after Chaplot *et al* [81].

3.3.2. Polaron formation. Polaron formation has been studied extensively for the Holstein model [72–77, 69, 78]. For noninteracting electrons, polaron formation is often associated with bipolaron formation [77, 78]. Since on-site bipolaron formation is strongly suppressed by the large on-site U relevant for cuprates, we focus on polaron formation here. We use $Z \to 0$ as the criterion for polaron formation. For the nearest neighbor Holstein model with a single electron and $\omega_{ph} = 0.0125W$ this was found to happen for $\lambda_c = 1.2$ [69], where W is the band width and λ is here defined as $\lambda = 2g^2/W$, corresponding to the assumption $N(0) = 1/W$ in equation (14). For the half-filled case with a semi-elliptical DOS and using the dynamical mean-field theory (DMFT) [79] it was found that $\lambda_c = 0.33$ [71], again using $\omega_{ph} = 0.0125W$ and putting $N(0) = 1/W$ in the definition of λ. Similar results were found by several other groups [75–78]. As in the weak coupling limit, there is a large difference between the single electron and half-filled cases [71].

To understand this difference, we consider polaron formation in the adiabatic limit by comparing free electron states with states of perfectly localized electrons [80, 71]. The energy for free electrons is $E_{free} = -4t$ per electron for the single electron case and $E_{free} = -16t/(3\pi) \approx -1.7t$ for the half-filled case. In the localized case, $E_{loc} = -g^2/\omega_{ph}$ per electron for both cases. For simplicity, we assume that polarons form when $|E_{loc}| > |E_{free}|$. This leads to a large $\lambda_c = 1$ for the single electron case and a much smaller $\lambda_c = 0.42$ for the half-filled case, in rather good agreement with more accurate calculations. The large difference between the two cases is due to the large difference in kinetic energy per electron. In the single electron case, the electron is at the bottom of the band and has the maximum (absolute) kinetic energy, while in the half-filled case the average kinetic energy is much smaller. The electron–phonon interaction energy can then win more easily and lead to polaron formation.

4. Experimental results

4.1. Phonon softening and width

There have been extensive studies of phonons in high-T_c cuprates using neutron scattering. For reviews, see, e.g., Pintschovius and Reichardt [5], Pintschovius [6], Egami and Billinge [31] and Egami [41]. Here we focus on results of particular interest for the EPI and in particular $La_{2-x}Sr_xCuO_4$, where the most complete results have been obtained. Figure 3 shows results of Chaplot *et al* [81] for undoped (left-hand side) and doped (right-hand side) $La_{2-x}Sr_xCuO_4$. The solid curves have been obtained within a shell model [81]. The shell model calculations give a rather accurate description of almost all phonon branches.

One striking exception is the highest mode of Δ_1 symmetry for doped systems. This is the so-called half-breathing phonon, which is a bond-stretching vibration of the oxygen atoms in the CuO_2 plane, as shown in figure 1. This phonon is rather well described by the shell model for the undoped system. However, doping leads to a strong softening half way along the (1, 0, 0) direction. This softening is anomalous in the sense that it is not captured by the shell model. A substantial softening is also found for the breathing phonon in the (1, 1, 0) direction, in particular for large dopings [5, 82]. Anomalies of such bond-stretching phonons have been observed by several groups for both high-T_c cuprates [83–85, 21, 86–89] and other compounds [90–92]. The anomalous behavior of this phonon is also illustrated by the large broadening in the doped system, as is shown in figure 4. Thus Pintschovius and Braden [21] found the FWHM intrinsic width for $\mathbf{q} = (0.5, 0, 0)$ to be 1.2 THz = 5 meV for 15% doping. Both the softening and the width indicate that this phonon couples strongly to doped holes. Using formula (equation (19)) of Allen [66, 67] for noninteracting electrons and the density of states $N(0) \sim 0.66$ states per eV and spin [93], the electron–phonon coupling can be estimated to

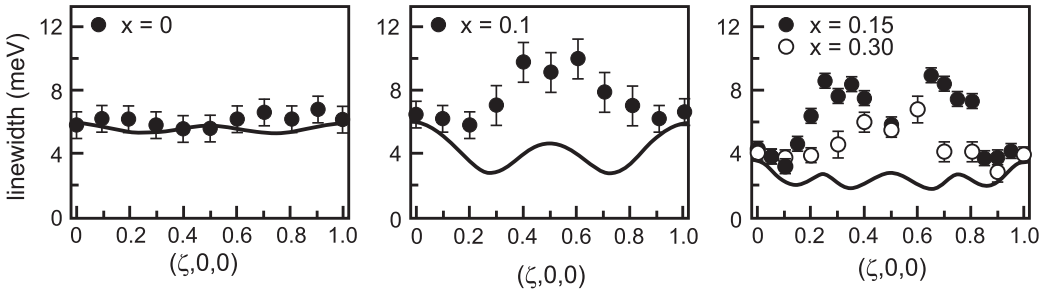

Figure 4. Width of the oxygen bond-stretching phonon for $La_{2-x}Sr_xCuO_4$ as a function of the reduced wavevector $(\zeta, 0, 0)$ and for doping $x = 0$ (left), $x = 0.1$ (middle) and $x = 0.15, 0.30$ (right). The full line shows the experimental resolution including focusing effects. The figure illustrates the large broadening for the doped system and the small intrinsic broadening for the undoped ($x = 0$) system (after Pintschovius [6]).

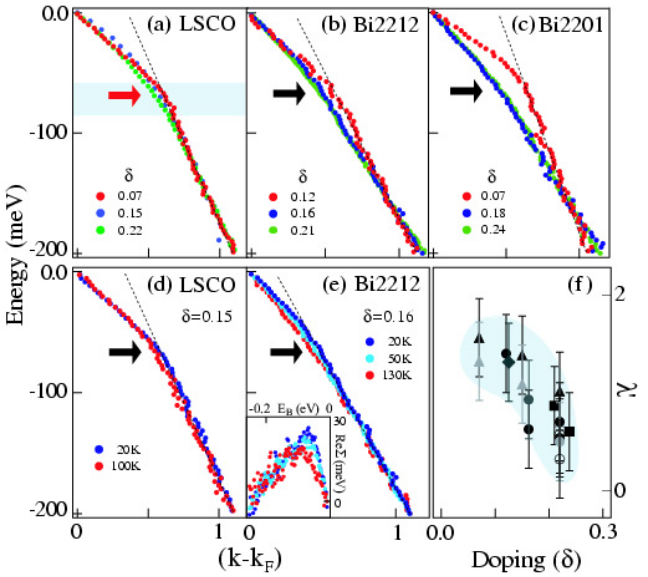

Figure 5. Dispersion in the $(0, 0)$–(π, π) direction for $La_{2-\delta}Sr_\delta CuO_4$ (LSCO), $Bi_2Sr_2CuO_6$ (Bi2201) and $Bi_2Sr_2CaCu_2O_8$ (Bi2212) for different dopings δ and temperatures T. The results in (a) and (b) were obtained for $T = 20$ K and in (c) for $T = 30$ K. The red arrow (in (a)) shows the energy of the $\mathbf{q} = (\pi, 0)$ half-breathing phonon and the black arrows the energies of the kinks. Panel (f) shows the change $1 + \lambda'$ of the slope at the kink (after Lanzara *et al* [8]).

be $\lambda \approx 0.1$–0.3 for the (half-) breathing phonons. In view of the arguments in section 5.1, in particular the discussion under equation (24), this estimate and similar estimates below should be taken with caution.

It is interesting to compare the (half-) breathing phonon with the $\mathbf{q} = (0.5, 0.5, 0)$ quadrupolar mode (where two of the O atoms around a Cu move towards the Cu and two O atoms move away from the Cu). While the (half-) breathing phonon is expected to couple strongly to the Zhang–Rice singlet, leading to a strong electron–phonon coupling, the quadrupolar mode does not couple to the singlet to lowest order, and it is expected to have a weak electron–phonon coupling. Indeed, the width of the quadrupolar mode is resolution limited [82]. This means that the width of the half-breathing phonon should be mainly due to the electron–phonon coupling, since defect scattering or other nonelectronic broadening mechanisms ought to influence the (half-) breathing and quadrupolar modes in similar ways.

Reznik *et al* [94] found a strong anomaly for the bond-stretching phonon around $\mathbf{q} = (0.25, 0, 0)$ for several cuprates. This anomaly was particularly large for systems with static stripe order but it was also seen for systems where stripe order has not been observed, e.g. superconducting $La_{2-x}Sr_xCuO_4$. This was interpreted in terms of a coupling to a dynamic charge inhomogeneity.

The O_Z^Z phonon of Λ_1 symmetry at about 17 THz in the undoped system and with the reduced wavevector (001) shows strong softening under doping (see figure 3). As shown to the right in figure 1, this phonon mainly involves the movement of apical O. The softening of this phonon was predicted by Falter *et al* [95, 96] before being observed experimentally. The width of the O_Z^Z phonon is 16 meV [5, 6], suggesting a very strong coupling to this mode.

There has also been a substantial interest in a B_{1g} phonon involving out-of-plane and out-of-phase vibrations of oxygen atoms in the CuO_2 plane. This phonon has an energy of about 42 meV for $YBa_2Cu_3O_{7-\delta}$. The phonon has been studied using both Raman [97–99, 53, 100, 57] and neutron scattering [54, 55]. This phonon shows an interesting change of frequency and width as the compound is cooled below T_c [97–99, 54, 55], and a Fano line shape is observed in Raman scattering [98, 99]. Fitting of the line shape and changes of the spectrum as the sample is cooled leads to estimates of the electron–phonon coupling in the range $\lambda \sim 0.02$–0.06 [53, 100, 57] for $YBa_2Cu_3O_{7-\delta}$, comparable to theoretical estimates, $\lambda = 0.02$, from band structure calculations [100] in the local density approximation. Qualitatively similar but smaller effects have also been observed for other phonons [54, 101].

4.2. Photoemission spectra

Photoemission spectra have been extensively reviewed [32, 36, 39, 40], and here we only show a few typical results of particular interest in the context of the EPI.

Much interest in the EPI has been created by the observation of a kink in the experimental electron dispersion for several cuprates [102–106, 8, 107, 108]. Some typical results are shown in figure 5. Lanzara *et al* [8] emphasized that such a kink is found for three different families of compounds (LSCO, Bi2201 and Bi2212), for different dopings and both below and above T_c. Other groups obtained similar results

for Bi compounds, but disagreed about whether there is a kink above T_c [107, 108] or not [105, 106]. The structure for LSCO, both below and above T_c, is more pronounced than for B2212 (see figure 5). For noninteracting electrons, the ratio of the slopes below and above the kink is expected to be given by the dimensionless electron–phonon coupling $1+\lambda$ (equation (17)). Figure 5(f) shows the change of slope $1+\lambda'$. Here λ' may be different from λ, since even the states at large binding energy may not show the 'bare' dispersion. If the theory for noninteracting electrons were applicable (equation (17)), this would suggest a coupling of the order of $\lambda \sim 1$.

While the early measurements showed only one kink at about 70 meV, later work found several structures at smaller binding energies [109, 110]. Estimates of Re $\Sigma(\mathbf{k}, \omega)$ were extracted from experiment by assuming that the underlying 'bare' dispersion is of second order in $|\mathbf{k}| - k_F$ over the range of interest. The second derivative of Re $\Sigma(\mathbf{k}, \omega)$ for $La_{2-x}Sr_xCuO_4$ then has structures at about 40–46 and 58–63 meV and possibly at 23–29 and 75–85 meV, suggesting that there is coupling to bosons at these energies.

The dispersion of the quasiparticle for $Bi_2Sr_2Ca_{n-1}Cu_nO_{2n+4}$ away from the nodal direction and, in particular, in the antinodal $(\pi, 0)$ direction has been extensively studied [111, 105, 107, 108, 112, 113]. For Bi2212 and Bi2223 below T_c there is a very strong structure away from the nodal direction. As discussed in section 3, if the kink is due to a coupling to a mode at energy ω_B, the kink is expected to appear at roughly $\omega_B+\Delta$ in the superconducting state [64, 114], where Δ is the gap. This suggests $\omega_B \approx 40$ meV for optimally doped Bi2212. The boson could be the B_{1g} buckling phonon mode [113], which has roughly the right energy. Alternatively, the coupling [112] could be to the so-called resonance peak, seen in inelastic neutron scattering in the superconducting states of Bi2212 and YBCO [115–118]. Recently, a broad structure has also been seen at 40–70 meV in the inelastic neutron scattering spectrum for $La_{2-x}Sr_xCuO_4$ [119].

4.3. Chemical potential. Polarons

A long-standing problem has been the position of the chemical potential in undoped or strongly underdoped cuprates as well as the interpretation of the PES spectra for these systems. Figure 6(a) shows the spectrum of undoped $Ca_2CuO_2Cl_2$ at the top of the band ($\mathbf{k} = (\pi/2, \pi/2)$). The spectrum has a broad feature centered at A and an onset at B. Figure 6(b) shows the dispersion of these features. The dispersion of A (figure 6(b)) agrees well with the extended t–J model [32]. It has therefore often been assumed that A represents a quasiparticle which is very strongly broadened by some unknown mechanism.

Shen *et al* [7] pointed out, however, that the peak shape is not Lorentzian, as would be expected from a lifetime broadening, but Gaussian. Even more seriously, a quasiparticle at the top of the valence band of an insulator cannot decay into an electron–hole pair, and one would expect the width to be small [7]. In figure 6(b), each horizontal line shows the chemical potential of a specific sample. Since the system is an insulator, one might expect the chemical potential to be pinned to impurities or defects and therefore depend on sample

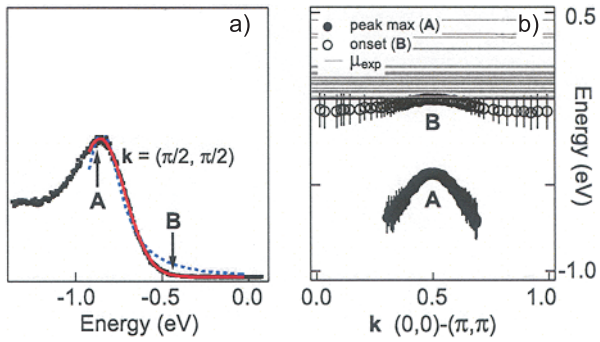

Figure 6. (a) The $\mathbf{k} = (\pi/2, \pi/2)$ spectrum of undoped $Ca_2CuO_2Cl_2$ as well as fits to a Gaussian (solid (red) curve) and a Lorentzian (dashed (blue) curve). The maximum of the broad feature is denoted by A and its onset by B. (b) Dispersion of A and B along the nodal direction as well as the different values of the chemical potential μ for a large number of samples (after Shen *et al* [7]).

preparation. The figure shows, however, that although the value of the chemical potential is highly sample dependent it is always at least about 0.45 eV above peak A. Shen *et al* [7] pointed out that all these puzzling features can be explained by assuming polaronic behavior due to strong coupling to bosons. Peak A is then a boson side band, explaining its large width and Gaussian shape, and B represents the quasiparticle, having too small a weight to be seen experimentally. This explains why the chemical potential is never lower than B in figure 6(b), since this is the top of the valence band in the new interpretation. It has furthermore been observed that the width of the broad peak increases substantially with T, providing further support to the interpretation in terms of coupling to bosons [120].

As the doping is increased, a quasiparticle is observed in $Ca_{2-x}Na_xCuO_2Cl_2$ for $x = 0.1$ [7]. The quasiparticle weight is small, however, and there is still much weight in the energy range of the side band. This suggests that the effects of the electron–boson interaction remain important for the doped system, although (small) polaronic effects are not seen anymore. For $La_{2-x}Sr_xCuO_4$ this is found to happen at smaller dopings ($x = 0.03$) [121], but it has been proposed that this could be due to phase separation [122].

4.4. Isotope effects

Isotope effects provide a good indication for electron–phonon interactions. In particular, the interest has focused on the superconductivity transition temperature T_c. A review of this work is given by Franck [9]. Generally, a small oxygen isotope effect was found for compounds having the composition which gives the highest T_c in that family. However, the isotope effect is often much larger for systems where T_c is suppressed by some substitutions.

Khasanov *et al* [123] observed an isotope effect in the penetration depth of nearly optimally doped $YBa_2Cu_3O_{7-\delta}$, using a muon-spin rotation technique, which allows a direct observation of the penetration. These results were interpreted in terms of an isotope effect in the carrier mass due to a strong electron–phonon interaction violating Migdal's theorem [123].

Gweon *et al* [124] studied the oxygen isotope effect on the PES spectra for optimally doped $Bi_2Sr_2CaCu_2O_{8+\delta}$ and found a very large effect, involving shifts as large as 30–40 meV. Douglas *et al* [125] in contrast found no large isotope effect, but concluded that their measurements are not inconsistent with a conventional isotope shift of the order of 3 meV. In later work they found that there is indeed such an isotope [127]. Gweon *et al* [126] argued that the difference between their results and the results of Douglas *et al* was due to the study of systems with different dopings.

4.5. Scanning tunneling spectroscopy

There has recently been much work based on scanning tunneling spectroscopy (STM), observing strong spatial modulations and a checkerboard structure [128–130, 10]. Of particular interest here is the work of Lee *et al* [10], studying $Bi_2Sr_2CaCu_2O_{8+\delta}$. From the second derivative of the tunneling current d^2I/dV^2 they determined the spatially dependent gap $\Delta(\mathbf{r})$ and the energy of a bosonic mode $\Omega(\mathbf{r})$ appearing in the spectrum. The mode energy showed the isotope effect expected for phonons involving primarily O atoms. Based on this and on the doping independence of $\Omega(\mathbf{r})$, it was concluded that the mode is an O phonon. Its average energy was found to be 52 meV, with a substantial spatial variation. They found anticorrelation between $\Omega(\mathbf{r})$ and $\Delta(\mathbf{r})$. They concluded that the results could be due to (i) a heterogeneity of the frequency and coupling constants of a pairing-related phonon causing a disorder in $\Delta(\mathbf{r})$, (ii) inelastic scattering of tunneling electrons by phonons unrelated to superconductivity [11] or (iii) a competing phase coupling to phonons and causing the anticorrelation between $\Omega(\mathbf{r})$ and $\Delta(\mathbf{r})$.

5. Interplay between Coulomb and electron–phonon interactions

In systems where the Coulomb repulsion U is important, the effects of the electron–phonon interaction can be strongly influenced. This can easily be seen for the Holstein–Hubbard model (equations (3) and (6)). The Hamiltonian can be transformed so that the phonons couple to the deviation of the site occupancies from their average. If U is small, the number of electrons on a given site fluctuates strongly, and there are substantial deviations from the average, even for a half-filled system. However, as U is increased, the fluctuations are reduced. For U large and close to half-filling, most sites then have exactly one electron. For these sites there is no electron–phonon coupling. This suggests that the effects of the electron–phonon coupling are strongly reduced as U is increased [131]. The problem is, however, substantially more complicated, as discussed below. For the cuprates, phonon frequencies are typically smaller than electronic energies. We therefore do not discuss the antiadiabatic limit, where phonon frequencies are much larger than electronic energies and quite different effects can be found [132, 78].

5.1. Sum rules

We first discuss the interplay between Coulomb and electron–phonon interactions in terms of sum rules for the imaginary parts of the electron and phonon self-energies. We consider the t–J model (equation (2)) and the electron–phonon coupling in equation (5) for $\mathbf{k}$-independent coupling $g(\mathbf{k}, \mathbf{q}) = g(\mathbf{q})$, which results in an on-site coupling.

5.1.1. Phonon self-energy. We first consider the phonon self-energy $\Pi(\mathbf{q}, \omega)$. This can be written as

$$\Pi(\mathbf{q}, \omega) = \frac{(g_{\mathbf{q}}^2/N)\chi(\mathbf{q}, \omega)}{1 + (g_{\mathbf{q}}^2/N)\chi(\mathbf{q}, \omega)D_0(\mathbf{q}, \omega)}, \tag{22}$$

where $\chi(\mathbf{q}, \omega)$ is the charge–charge response function and $D_0(\mathbf{q}, \omega)$ is the free phonon Green's function. Khaliullin and Horsch [46] showed that this function satisfies a sum rule (at $T = 0$)

$$\frac{1}{\pi N}\sum_{\mathbf{q}\neq 0}\int_{-\infty}^{\infty} |\operatorname{Im}\chi(\mathbf{q}, \omega)|\, d\omega = 2\delta(1-\delta)N, \tag{23}$$

where δ is the doping. This result is suppressed by a factor $2\delta(1-\delta)$ compared with the result for noninteracting electrons in a half-filled band. Since $\chi(\mathbf{q}, \omega)$ becomes small for small δ, the denominator in equation (22) is not very important, and the sum rule in equation (23) also applies approximately to $\Pi(\mathbf{q}, \omega)/g_{\mathbf{q}}^2$ [133]

$$\frac{1}{\pi N}\sum_{\mathbf{q}\neq 0}\frac{1}{g_{\mathbf{q}}^2}\int_{-\infty}^{\infty} |\operatorname{Im}\Pi(\mathbf{q}, \omega)|\, d\omega \approx 2\delta(1-\delta). \tag{24}$$

Since typically $\delta \sim 0.1$, this implies that the softening and width of a phonon due to the creation of electron–hole pairs is drastically reduced. A formula of Allen [66, 67] is often used to estimate the electron–phonon coupling λ from the phonon width $2\operatorname{Im}\Pi(\mathbf{q}, \omega)$. This formula is derived for noninteracting electrons and it neglects the strong reduction of Π in equation (24). Its use for high-T_c cuprates may therefore substantially underestimate λ.

5.1.2. Electron self-energy. To derive a similar sum rule for the electron self-energy, we define a Green's function

$$G(\mathbf{k}, z) = \frac{a_{\mathbf{k}}}{z - \varepsilon_{\mathbf{k}} - \Sigma(\mathbf{k}, z)}, \tag{25}$$

where $a_{\mathbf{k}}$ is a weight and $\Sigma(\mathbf{k}, z)$ is the electron self-energy. The z-independent part of Σ is included in the energy $\varepsilon_{\mathbf{k}}$, so that $\Sigma(\mathbf{k}, z) \sim b_{\mathbf{k}}/z$ for large z. By studying the large z behavior of $G(\mathbf{k}, z)$ and $\Sigma(\mathbf{k}, z)$, Rösch and Gunnarsson [133] related a sum rule for $\Sigma(\mathbf{k}, z)$ to moments of the electron–phonon interaction part of the Hamiltonian. For the t–J model and $\delta = 0$, the sum rule takes a very simple form

$$\frac{1}{\pi}\int_{-\infty}^{0} \operatorname{Im}\Sigma_{\mathrm{ep}}(\mathbf{k}, \omega - i0^+)\, d\omega = \frac{1}{N}\sum_{\mathbf{q}} |g_{\mathbf{q}}|^2 \equiv \bar{g}^2, \tag{26}$$

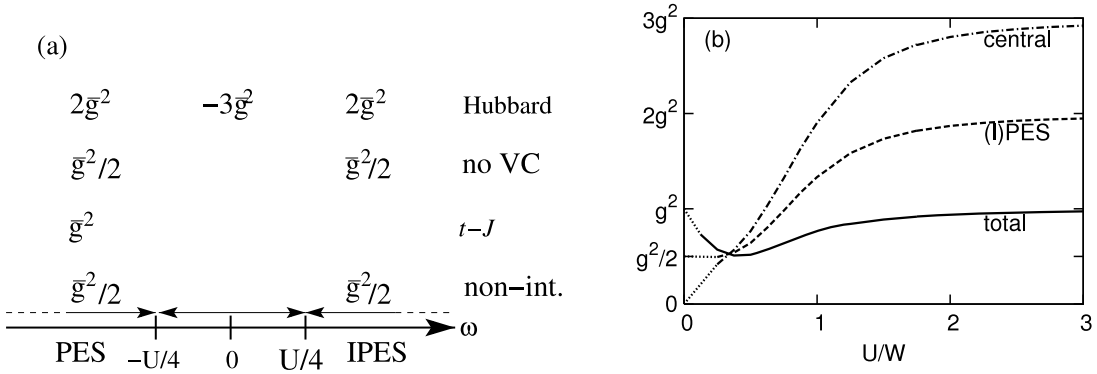

Figure 7. (a) Weights obtained by integrating $\mathrm{Im}\,\Sigma_{\mathrm{ep}}(\mathbf{k}, \omega - \mathrm{i}0^+)/\pi$ over the indicated frequency intervals for the half-filled Hubbard and undoped t–J models. Also shown are the results for the Hubbard model without vertex corrections (no VC) and the lowest-order ($\mathbf{k}$-averaged) result for the $U = 0$ Hubbard model (non-int.). For the t–J model, the photoemission spectrum has been shifted by $-U/2$ and for the $U = 0$ Hubbard model the PES and inverse PES (IPES) spectra have been shifted by $-U/2$ and $U/2$, respectively. (b) U dependence of the absolute value of the total and partial sum rules for $\mathrm{Im}\,\Sigma_{\mathrm{ep}}$ using DMFT with $\lambda = 0.0025$. The dotted lines indicate the expected small $-U$ behavior. W is the $U = 0$ band width (after Rösch *et al* [134]).

where Σ_{ep} is the difference in self-energy for the system with and without EPI. Since the inverse photoemission (IPES) spectrum has zero weight for $\delta = 0$, the integration extends only to $\omega = 0$. This result is shown in figure 7(a). For noninteracting electrons and to lowest order (in $g_{\mathbf{q}}^2$), a similar sum rule for $|\,\mathrm{Im}\,\Sigma_{\mathrm{ep}}(\mathbf{k}, \omega - i0^+)|$ (averaging over $\mathbf{k}$) gives the right-hand side $\bar{g}^2/2$ for integration up to $\omega = 0$ or $\bar{g}^2$ for integration over all energies (see figure 7(a)). Thus the effect of the electron–phonon coupling is strongly reduced by the small doping for the phonon self-energy but not for the electron self-energy, at least not in a sum rule sense.

The sum rule in equation (26) can be understood as follows. The electron Green's function describes the creation of a hole (or an electron). The phonons couple strongly to the charge of this hole, even if charge fluctuations are strongly suppressed elsewhere in the system. On the other hand, if a phonon is created, there is only a small fraction δ of singlets that can respond. As a result, the electron–phonon interaction can be expected to appear to be a factor of $1/(c\delta)$ stronger in $\mathrm{Re}\,\Sigma(\mathbf{q}, \omega)$ than in $\mathrm{Im}\,\Pi(\mathbf{q}, \omega)$ (phonon width), where $c \sim$ 2–4 depends on the assumptions about the ω-dependencies of $\mathrm{Im}\,\Sigma$ and $\mathrm{Im}\,\Pi$.

Although the arguments above show that the sum rule (26) should not go to zero for $\delta \to 0$, the result is, nevertheless, nontrivial. The derivation depends on the coupling being on-site and we have found no simple result for an off-site coupling. The right-hand side is independent of $\mathbf{k}$, t and J and it remains proportional to $\bar{g}^2$ even for large $\bar{g}$.

Similar results can be derived for the half-filled Hubbard model in the large U limit [134]. The PES spectrum is expected to be close to the result for the t–J model, but the sum rule differs by a factor of two, due to the different integrated weights of the total (PES and IPES) spectra of the two models (see figure 7(a)). Integrating $\mathrm{Im}\,\Sigma_{\mathrm{ep}}(\mathbf{k}, \omega - \mathrm{i}0^+)/\pi$ over all frequencies for the large U Hubbard model gives the sum rule $\bar{g}^2$. Therefore, there is a contribution $-3\bar{g}^2$ close to $\omega = 0$, showing how the EPI reduces a large positive contribution at $\omega = 0$ already present for $\bar{g} = 0$. Going from $U = 0$ to large U, the sum rules for the PES or IPES part increase by a factor of four. This is illustrated in figure 7(b). Interestingly, a substantial part of this change has already happened when U is comparable to the $U = 0$ band width W [134]. The phonon sum rule is further illustrated in section 6.1.

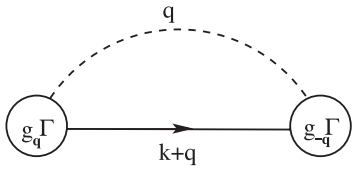

Figure 8. Contribution to Σ_{ep}. The full and dashed lines are electron and phonon Green's functions, respectively, and the circle is a vertex correction.

5.2. *Vertex corrections*

In a diagrammatic language, an important contribution to Σ_{ep} is shown in figure 8, expressed in terms of a vertex correction Γ. Figure 7(a) shows that the neglect of Γ (no VC) in the half-filled large U Hubbard model leads to a large violation of the sum rules in the previous section. It is therefore interesting to study vertex corrections [135–137, 33, 138–141].

In particular, Kulic and Zeyher [135, 137] have argued that in the large U limit vertex corrections favor small angle scattering over back-scattering. This would have the important effect of favoring d-wave superconductivity. Huang *et al* [138] performed a determinantal quantum Monte Carlo (QMC) calculation [142] for the Holstein–Hubbard model for an 8×8 cluster for $T = 0.5$, where the hopping integral was $t = 1$ and the band width $W = 8$. The occupancy was $n = 0.88$. They defined an effective coupling

$$g(p, q) = \Gamma(p, q)\sqrt{Z(p)Z(p+q)}, \tag{27}$$

where $\Gamma(p, q)$ is the vertex correction, p and $p + q$ stand for the momenta and imaginary frequencies of the incoming and outgoing electrons, respectively, and Z is the quasiparticle

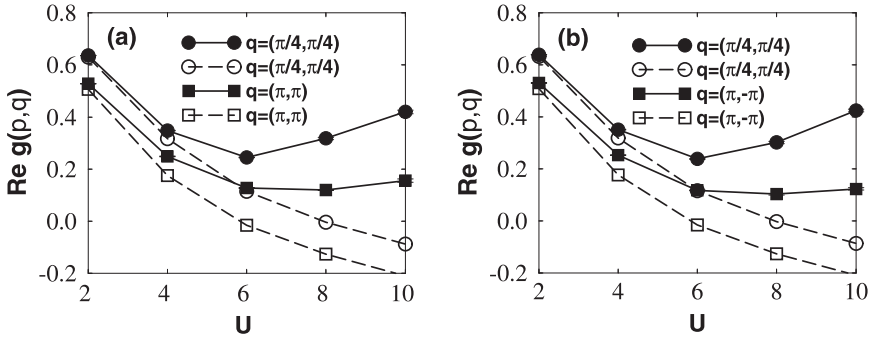

Figure 9. Real part of $g(p, q)$ as a function of U for (a) $\mathbf{p} = (-\pi, 0)$ and (b) $\mathbf{p} = (-\pi/2, \pi/2)$. The value of $\mathbf{q}$ is indicated by the shape of the symbol. The solid circles are Monte Carlo results and the open symbols show results from perturbation theory (after Huang *et al* [138]).

weight. The frequencies were put at their minimum value πT. Results are shown in figure 9. It illustrates how $g(p, q)$ is reduced relative to its $U = 0$ value for all parameters shown, due to the reduction of the quasiparticle weights Z. Small angle scattering [$\mathbf{q} = (\pi/4, \pi/4)$], however, is favored over back-scattering [$\mathbf{q} = (\pi, \pi)$] for large values of U, which helps d-wave superconductivity. Some questions have been raised related to the large value of T which has to be used in the QMC calculations [139, 140].

5.3. Effects due to antiferromagnetic correlations

Equation (26) shows that $\mathrm{Im}\,\Sigma_{\mathrm{ep}}(\mathbf{k}, \omega)$ is not suppressed by correlation effects in a sum rule sense. The sum rule does not tell us, however, how the contributions are distributed in frequency. Correlation effects tend to reduce the dispersion and provide more low-lying excitations to which a quasiparticle could couple. This tends to increase $\mathrm{Re}\,|\Sigma_{\mathrm{ep}}(\mathbf{k}, \omega)|$. On the other hand, spectral weight is removed from the quasiparticles and shifted away from the Fermi energy by correlation effects. This tends to have the opposite effect. These two effects need not cancel, as discussed below.

5.3.1. Exact diagonalization. There have been a large number of studies of the Holstein–Hubbard, Holstein–t–J or related models based on exact diagonalization [143–150, 70, 151, 152]. Here we show some typical results. Zhong and Schüttler [144] studied a Holstein–Hubbard model $H_{\mathrm{Hub}}+H_{\mathrm{Hol}}$ (equations (3), (6)) in the adiabatic limit ($\omega_{\mathrm{ph}} = 0$) using exact diagonalization for an eight-site ($\sqrt{8} \times \sqrt{8}$) cluster with one doped hole, i.e. seven electrons. They found that the system goes from a delocalized state to a polaronic state for $\lambda \approx 0.2$–0.4 in the range $U/t \approx 8$–12. This was compared with a calculation for a spin-polarized system with one hole, where the antiferromagnetic spin correlations are removed. In this case the transition to a polaronic state occurred for $\lambda \approx 0.96$. This was interpreted in terms of antiferromagnetic correlations strongly reducing the coupling λ needed to obtain polaronic behavior. Similar conclusions were obtained for a larger cluster and using small but finite phonon frequencies by Fehske *et al* [147, 148, 150], who studied Holstein–t–J and Holstein–Hubbard clusters. These calculations showed that the adiabatic approximation overestimates the tendency to (small) polaron formation. The quasiparticle weight and dispersion were shown to be reduced as the coupling was increased. Bäuml *et al* [150] studied the optical conductivity and argued that the mid-infrared peak in cuprates is mainly of electronic origin while it is mainly of polaronic origin in nickelates. Optical experiments for cuprates have, however, also been interpreted in terms of polarons [24–29].

5.3.2. Self-consistent Born approximation. Ramsak *et al* [68] used a self-consistent Born approximation (SCBA) [153–157] for a Holstein–t–J model, where a hole is assumed to couple to magnons and phonons. The problem is treated in a diagrammatic approach, neglecting crossing phonon or magnon lines. The electron–phonon part of the self-energy was written as

$$\Sigma_{\mathrm{el-ph}}(\mathbf{k}, \omega) = \frac{1}{N} \sum_{\mathbf{q}} g_{\mathbf{q}}^2 G(\mathbf{k} - \mathbf{q}, \omega - \omega_{\mathrm{ph}}), \qquad (28)$$

where N is the number of sites, $g_{\mathbf{q}}$ a coupling constant, $G(\mathbf{k}, \omega)$ the electron Green's function and ω_{ph} the phonon frequency. Equation (28) assumes that the electron–phonon coupling is not very strong and it neglects an indirect contribution, $\Delta\Sigma_m$ [158], via the coupling of magnons to the changes of the Green's function due to the electron–phonon coupling. To interpret their calculation, Ramsak *et al* [68] argued that the main contribution to $\Sigma_{\mathrm{el-ph}}$ is due to the coherent part $G_{\mathrm{coh}}(\mathbf{k}, \omega) = Z(\mathbf{k})/(\omega - \varepsilon_{\mathbf{k}})$ of the Green's function, where $Z(\mathbf{k})$ is the quasiparticle weight. They furthermore assumed that the quasiparticle energy $\varepsilon_{\mathbf{k}}$ in the absence of phonons can be parameterized in terms of effective masses $m_{\parallel}$ and $m_{\perp}$, i.e., $\varepsilon_{\mathbf{k}} \approx \tilde{\varepsilon}_{\mathbf{k}} = k_{\parallel}^2/2m_{\parallel} + k_{\perp}^2/2m_{\perp}$, where $k_{\parallel}$ and $k_{\perp}$ are measured from $(\pi/2, \pi/2)$ in the $(\pi/2, \pi/2) \rightarrow (0, 0)$ and $(\pi/2, \pi/2) \rightarrow (\pi, 0)$ directions, respectively. This gives

$$\Sigma_{\mathrm{el-ph}}(\mathbf{k}, \omega) = 4\frac{1}{(2\pi)^2} \int \mathrm{d}^2 q \frac{Z(\mathbf{k} - \mathbf{q}) g_{\mathbf{q}}^2}{\omega - \omega_{\mathrm{ph}} - \tilde{\varepsilon}_{\mathbf{k}-\mathbf{q}}}, \qquad (29)$$

where the factor of four is due to the presence of four hole pockets at $(\pm\pi/2, \pm\pi/2)$ and the q-integrations over the surroundings of a hole pocket have been extended to infinity. This leads to a simple approximate formula for the

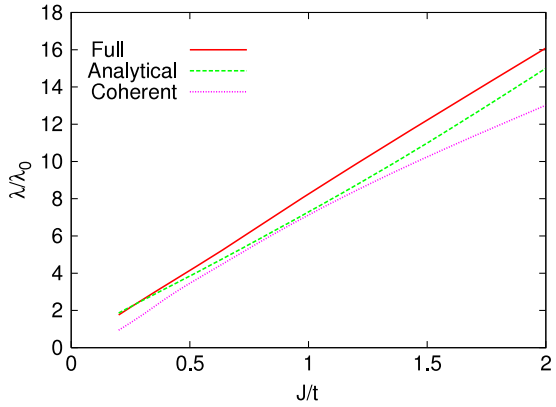

Figure 10. λ/λ_0 as a function of J/t for $\omega_{\rm ph}/t = 0.1$ and $g/t = 0.1$. The result of the SCBA (full line) is compared with the contribution from the coherent part of the Green's function (dashed) and the analytical formula (30) (after Gunnarsson and Rösch [158]).

enhancement of the mass m^* in the $(\pi/2, \pi/2) \rightarrow (0, 0)$ direction due to the electron–phonon interaction,

$$\frac{m^*}{m_\parallel} = \left(1 - 4\lambda_0 Z^2 \frac{\sqrt{m_\parallel m_\perp}}{m_0}\right)^{-1} \equiv (1 + \lambda), \qquad (30)$$

where Z is approximated by $Z(\pi/2, \pi/2)$, λ_0 (equation (21)) is the λ obtained for a Holstein model with just one electron at the bottom of the band and $m_0 = 1/|2t|$ is the corresponding mass. Equation (30) contains an extra factor Z [158], obtained from solving the Dyson equation for the quasiparticle energy with electron–phonon interaction. As shown in figure 10, equation (30) then agrees rather well with the full calculation for a large range of J/t values. The figure illustrates that the use of the coherent part (equation (29)) is a rather good approximation for large J/t, while for small J/t it substantially underestimates λ, primarily due to the neglect of $\Delta\Sigma_m$.

The expression for $m^*/m_\parallel$ in equation (30) is reduced by Z^2 but enhanced by the large effective mass factor $\sqrt{m_\parallel m_\perp}/m_0$, representing the reduced mobility of the carriers due to antiferromagnetic correlations. Thus the antiferromagnetic correlations greatly help polaron formation [68]. For large J/t, the net effect is an increase of λ/λ_0. For $J/t = 0.3$, the factor $Z^2\sqrt{m_\parallel m_\perp}/m_0$ is actually smaller than unity, but λ/λ_0 is still enhanced, due to the factor of four in equation (30), resulting from the four hole pockets.

5.3.3. Quantum Monte Carlo calculations. Mishchenko and Nagaosa [69] studied an undoped infinite Holstein–t–J model using a diagrammatic Monte Carlo method. In contrast to the treatment above, they included diagrams with crossing phonon propagators and only neglected diagrams with magnon propagators crossed by phonon or other magnon propagators. Using the parameters $\omega_{\rm ph}/t = 0.1$ and $J/t = 0.3$, they found self-trapping for $\lambda \approx 1.2$ for an electron at the bottom of the band in the Holstein model but already for $\lambda \approx 0.4$ in the Holstein–t–J model [69]. It was concluded that the antiferromagnetic ground state and the coupling to magnons help the formation of polarons.

5.3.4. Dynamical mean-field calculations. Polaron formation has been extensively studied in the dynamical mean-field theory (DMFT) [79], which becomes exact for infinite degeneracy. Cappelluti and Ciuchi [159] developed a method for analytically solving the Holstein–t–J model in this limit. They found that antiferromagnetic correlations and the electron–phonon interaction mutually reinforce each other. Cappelluti *et al* [160] studied the relation between polaron formation and structures in the optical conductivity. Somewhat similar work has also been done using other methods [27, 29]. The T dependence of the optical conductivity sum rule was studied by Toschi and Capone [161] using DMFT. It was shown that the temperature scale is strongly renormalized by strong correlation.

The Holstein–Hubbard model in the paramagnetic phase has been studied extensively using the DMFT method (P-DMFT) [162, 163, 132]. It was shown that in the P-DMFT the electron–phonon interaction is strongly suppressed by the Coulomb interaction, in the sense that polaron formation is suppressed and states close to the Fermi energy are not strongly influenced by the EPI. The main effect was found to be a renormalization of U. As shown in section 5.5, allowing for antiferromagnetic (AF) correlations by using an AF–DMFT method greatly increases the importance of the electron–phonon interaction.

5.4. Differences between different phonons

Sakai *et al* [149] considered coupling via hopping integrals (in a three-band model) to breathing and buckling phonons involving in-plane and out-of-plane movements, respectively, of O atom in the CuO_2 plane. By transforming to a t–J model, they obtained an on-site electron–phonon coupling

$$H_{\rm BB} = \omega_{\rm ph} \sum_{i,\delta} b^\dagger_{i\delta} b_{i\delta} + g \sum_{i,\delta} (b_{i,\delta} + b^\dagger_{i,\delta})(n_i \mp n_{i+\delta}), \qquad (31)$$

where i labels the Cu sites and $\delta = x, y$ differentiates the two bond directions. The minus sign between the two occupation numbers refers to a breathing phonon and the plus sign to a buckling phonon. For a breathing phonon, an O atom between two Cu atoms moves towards one Cu atom and thereby away from the other Cu atom, influencing Zhang–Rice singlets centered around the two Cu sites in opposite ways, as described by the minus sign in equation (31). A buckling mode leads to a movement perpendicular to the CuO_2 plane of a O atom, which influences the two neighboring Cu sites in the same way, giving a plus sign in equation (31). The coupling to buckling phonons vanishes to linear order for a single perfect CuO_2 plane, but it is finite for a plane with a static buckling.

Figure 11 shows the kinetic energy $E_{\rm kin}$ as a function of the coupling constant g for breathing and buckling phonons. The figure illustrates that as g is increased $|E_{\rm kin}|$ is more rapidly reduced for breathing than buckling phonons. If a (local) breathing phonon is excited, the potential is lowered on one site but increased on a neighboring site. This tends to strongly inhibit hopping and reduce $|E_{\rm kin}|$. Exciting a buckling phonon, on the other hand, lowers the potential on both sites involved, and this inhibits hopping less. This illustrates the importance of what type of phonons the electrons couple to.

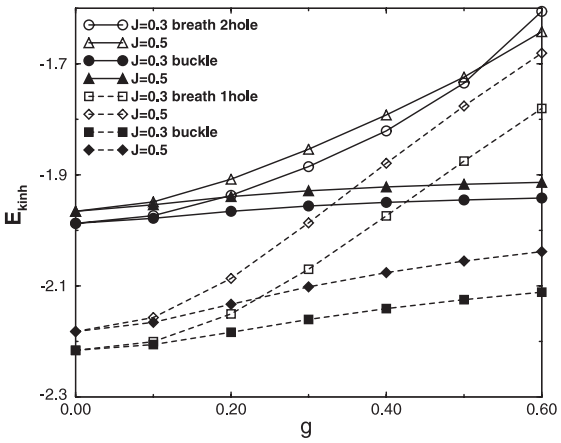

Figure 11. Kinetic energy $E_{\rm kin}$ per hole as a function of coupling g for a Cu_8O_{16} cluster with $\omega_{\rm ph} = 0.2$. All energies are in units of the hopping integral t. Open (solid) symbols correspond to the breathing (buckling) phonon. Solid (dashed) lines refer to two (one) doped hole(s). The figure shows how the breathing phonons reduce hopping more efficiently than buckling phonons (after Sakai *et al* [149]).

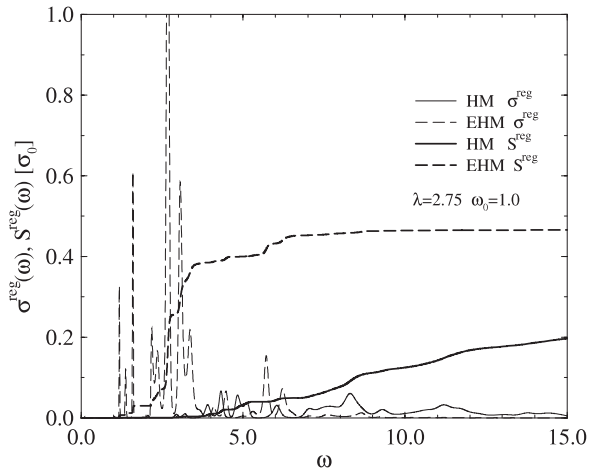

Figure 12. Optical conductivity $\sigma^{\rm reg}(\omega)$ (thin lines) and sum rule $S^{\rm reg}(\omega)$ (thick lines) for the 1D Holstein (HM) and extended Holstein (EHM) models in the strong coupling limit (after Fehske *et al* [70]).

Fehske *et al* [70] observed similar effects when comparing the one-dimensional Holstein model (HM) to an extended Holstein model (EHM) with a Fröhlich type long-ranged electron–phonon coupling decaying as $1/d^3$ for large d, where d is the distance between the electron and a phonon. Figure 12 shows the optical conductivity $\sigma^{\rm reg}(\omega)$ for the EH and EHM as well as the sum rule $S^{\rm reg}(\omega) = \int_0^\omega {\rm d}\omega' \sigma^{\rm reg}(\omega')$, where the Drude peak has been removed from $\sigma^{\rm reg}(\omega)$. The optical conductivity is determined by the current–current correlation function, where the current operator for the present models corresponds to the transfer of an electron to a neighboring site. In the strong coupling limit, an electron in the HM has a large binding energy, $\varepsilon_{\rm p}$, essentially due to phonons on the same site. If the electron is moved to a neighboring site by the current operator, it loses the energy $\varepsilon_{\rm p}$ and it leaves behind excited phonons with the energy $\varepsilon_{\rm p}$. Therefore, $\sigma(\omega)$ tends to have a broad peak centered at $2\varepsilon_{\rm p}$, which is at $\omega = 11$ in figure 12 [70]. Due to the long-range of nature of the phonons in the EHM, phonons relatively far away from the electron are excited in the EHM, even in the strong coupling limit. Moving an electron to a neighboring site then costs much less energy, and $\sigma(\omega)$ has a peak at a much smaller energy [70]. Coupling to breathing phonons should instead shift the peak in $\sigma(\omega)$ to higher energies than in the Holstein model for a given λ.

There is a substantial coupling to apical oxygen phonons [5, 23], in particular to modes with a small $\mathbf{q}$-vector parallel ($\mathbf{q}_\parallel$) to the CuO_2 plane. These phonons should have a similar effect to the phonons in the EHM model above, while modes with $|\mathbf{q}_\parallel| \sim \pi/a$ should be more similar to a breathing phonon.

5.5. *Effects of Coulomb interaction*

Most of the work above used the Holstein–t–J or large U Holstein–Hubbard model and focused on the effects of antiferromagnetic (AF) correlations. Here we focus on the Holstein–Hubbard model, which allows a continuous increase of U and also to study other effects of U.

In section 5.3.4, it was found that treating the paramagnetic state in DMFT (P-DMFT) leads to a strongly suppressed EPI. Due to the nature of P-DMFT, antiferromagnetic (AF) correlations are suppressed, which have been found to be important for the EPI (see section 5.3). This suggests that it would be interesting to apply an AF–DMFT method, where an AF state is allowed. A second reason for this is that the half-filled Holstein–Hubbard model must be an insulator for large U. In the P-DMFT this can only happen via $Z \to 0$. From equation (30) it follows that this strongly suppresses the EPI, at least in the weak coupling limit. In the AF–DMFT, on the other hand, it is possible to have an insulating state with $Z > 0$. A third reason is to notice that P-DMFT is equivalent to solving an Anderson impurity model (with a self-consistent host). We consider the electron Green's function, describing, for instance, the removal of an electron in photoemission. We focus on the corresponding final states close to the Fermi energy, i.e. in the Kondo resonance. These states have essentially the same occupancy of the local level as the ground state, since the electron removed in the photoemission process is replaced by an electron hopping in from the host [164]. Actually, in the limit of infinite orbital degeneracy and an infinite U, the occupancy of the local level is unchanged [165]. Seen from the phonons, coupling to the net charge of the local level, a photoemission process corresponding to the Kondo peak then leads to no change. As a result, Holstein phonons have only an indirect influence on these states due to a renormalization of the parameters [164, 162]. In the Holstein–Hubbard model, however, an electron filling the hole created in photoemission comes from another 3d level, which also couples to phonons, and in general this may be expected to influence the spectrum also close to the Fermi energy.

The AF–DMFT method has been applied to the Holstein–Hubbard model on a Bethe lattice using exact diagonalization for solving the impurity problem [71]. The results for Z are shown in figure 13. The results for $U = 0$ show how

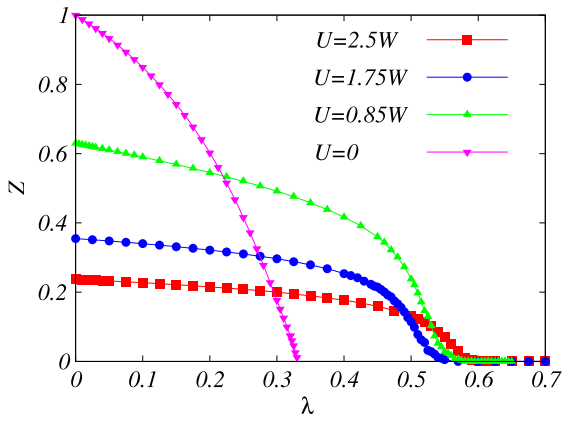

Figure 13. Z as a function of λ for different U and for $\omega_0 = 0.0125W$, where W is the band width. The figure shows how the Coulomb interaction moderately suppresses polaron formation ($Z \to 0$) (after Sangiovanni *et al* [71]).

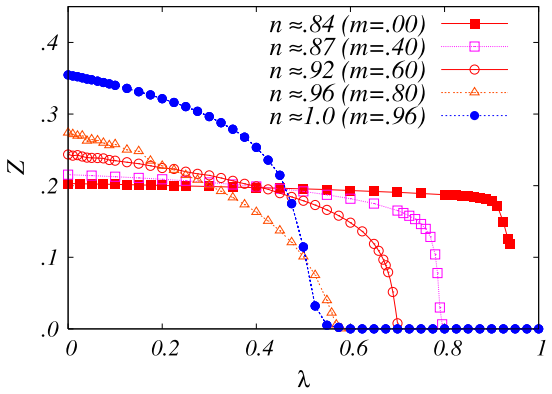

Figure 15. Z as a function of λ for different magnetic moments m and associated fillings n for $U = 1.75W$ and $\omega_0 = 0.0125W$. The figure illustrates how the critical λ_c is increased as the filling is reduced (doping is increased) due to a reduction of antiferromagnetic correlations (after Sangiovanni *et al* [71]).

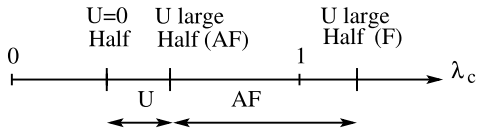

Figure 14. Critical value λ_c for polaron formation ($Z \to 0$) in the half-filled Holstein model ($U = 0$) as well as in the large U Holstein–Hubbard model in the antiferromagnetic (AF) or ferromagnetic (F) states. The figure illustrates that AF correlations help the EPI (smaller λ needed for polaron formation) but that the net effect of U is a moderate suppression of the EPI.

Z is reduced from $Z = 1$ for $\lambda = 0$ to $Z \approx 0$ for $\lambda = \lambda_c = 0.33$. We use this as the criterion for (small) polaron formation. For $\lambda = 0$, an increase of U leads to a decrease of Z. However, Z decreases more slowly with λ for a finite U, and polaron formation happens at a somewhat larger value λ_c. Thus the Coulomb interaction moderately suppresses polaron formation, at least in AF–DMFT. This is also shown in figure 14.

It is important to notice that in the half-filled large U case there is no polaron formation in the ground state, since U suppresses charge fluctuations. The Green's function describes the final state after an electron has been removed (in, e.g., photoemission) and $Z \to 0$ describes how the corresponding hole localizes due to polaronic effects. This is different from the Holstein model, where polaron formation means the formation of polarons also in the ground state.

Macridin *et al* [166] performed a dynamical cluster calculation (DCA) for the Holstein–Hubbard model using a 2×2 cluster. Using a different definition of polaron formation, they found $\lambda_c \gtrsim 0.5$, similar to the result in figure 13. They emphasized the synergistic cooperation between the EPI and AF correlations. As a result they found that the AF transition temperature at finite doping is enhanced by the EPI. Macridin *et al* [166] and Fu *et al* [167] pointed out that the EPI can contribute to a charge density modulation seen experimentally.

To see the effects of the antiferromagnetic correlations we compare with polaron formation in the ferromagnetic state (F in figure 14), where antiferromagnetic correlations are completely suppressed. We then find that λ_c is very large. When the antiferromagnetic correlations are reintroduced, λ_c is strongly reduced (see figure 14), meaning that the electron–phonon coupling becomes more efficient, as expected.

Although the antiferromagnetic effects, caused by U, strongly reduce λ_c, the net effect of U is still an increase of λ_c, due to other effects of U. We may then ask what this is due to. The Green's function of the ferromagnetic half-filled state describes the creation of a hole in an otherwise filled spin up band. In the absence of phonons, this hole could move completely freely, and if the system has electron–hole symmetry this state is equivalent to a Holstein model with a single electron at the bottom of the band. The half-full Holstein model and the single electron Holstein model were compared in section 3.3. It was shown that λ_c is much larger in the single electron case, because the absolute value of the hopping energy per electron is much larger. Counter-intuitively, λ_c is therefore larger for the ferromagnetic Holstein model than for the half-filled Holstein model because the hopping energy of the hole to be localized in the ferromagnetic case is larger, although the total hopping energy is strongly suppressed.

The AF–DMFT calculation can also be applied to the doped system. Figure 15 shows Z as a function of λ for different fillings n. As the filling is reduced (doping increases) the critical λ_c for polaron formation increases. The reason is that AF correlations decrease with increasing doping, which reduces the effects of the EPI. This is consistent with the experimental observation [7] that polaron formation is gradually suppressed as the system is doped. In addition to the effect discussed here, the calculated strong coupling to apical oxygen phonons [23] becomes more efficiently screened as the system is doped, also reducing the tendency to polaron formation.

5.6. Coupling constants

Above we have discussed extensively how the EPI is influenced by the Coulomb interaction and antiferromagnetic correlations

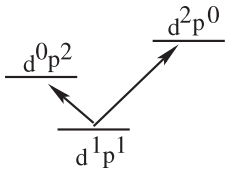

Figure 16. Configurations involved in the formation of the Zhang–Rice singlet.

by comparing the Holstein–t–J or Holstein–Hubbard models with the Holstein model, assuming that the coupling constants remain the same as U is increased. As discussed below, however, the coupling constants themselves can change in an essential way.

5.6.1. Breathing phonons. Starting from a three-band model [42], a t–J model with phonons can be derived [51]. A similar derivation can be made for the case when $U = 0$ by projecting out the oxygen 2p states. The EPI is different in the two cases, due to the formation of a Zhang–Rice singlet in the large U case. The coupling to a singlet involves extra prefactors. The main reason for the difference, however, is illustrated in figure 16. The undoped ground state is nominally a d^1 state in the hole picture. Doping adds a 2p hole, nominally leading to a d^1p^1 configuration. This configuration couples to two configurations, d^0p^2 and d^2p^0. The corresponding projection (Löwdin downfolding) for the $U = 0$ case only results in the coupling to one configuration [22]. The two coupling possibilities in the large U case lead to an enhancement in the coupling constant squared of the order of three. In addition the coupling is screened in the $U = 0$ case, which reduces the coupling by an additional factor of about two [22]. This suggests that many-body effects are crucial for the coupling to the breathing phonons.

5.6.2. Apical oxygen phonons. Neutron scattering experiments [5] and calculations [23] suggest that there is a strong coupling to apical oxygen phonons. This strong coupling was found [23] to depend crucially on the poor screening in these systems, in particular for the undoped system, being an insulator. This was studied further by Meevasana *et al* [110, 168]. They extracted the effective EPI for optimally doped Bi2201 from the structures of the PES spectrum in the nodal direction and compared this with the experimental loss function in the c-direction, obtained from optical measurements. A rather good agreement was found and it was concluded that an essential part of the coupling is due to c-axis O phonons. For the overdoped sample, they then argued that phonons below an energy of the order of 60 meV are screened and do not essentially contribute to the EPI. The result is then a reduction of the coupling and a stronger emphasis on high-lying phonons, in agreement with the EPI extracted from experiments for overdoped Bi2201.

6. Phonon spectral function

6.1. Phonon softening

The softening of the (half-) breathing phonon has been studied by several groups [45–51]. Von Szczepanski and Becker [45] derived a t–J model with phonons starting from a three-band model. They calculated the density response function for the electronic system using exact diagonalization for a small cluster and from this the phonon self-energy and softening. Khalliulin and Horsch [46–49] calculated the density response of the t–J model using both slave bosons [46] and slave fermions [48], from which they deduced the phonon self-energy. Their calculated relative softening for the half-breathing [$\mathbf{q} = (\pi, 0)$] and breathing [$\mathbf{q} = (\pi, \pi)$] phonons are compared with experiment in figure 17. The theory correctly predicts that for intermediate dopings the half-breathing [$\mathbf{q} = (\pi, 0)$] phonon is softened more than the breathing phonon, although the coupling constant is larger for the breathing phonon (equation (6)). For large dopings ($\delta \approx 0.3$) the softenings of the two modes become comparable. This was predicted before the experiment had been done.

Rösch and Gunnarsson [51] derived a t–J model with phonons starting from a three-band model. Using input from *ab initio* calculations they obtained the electron–phonon coupling. The t–J model was solved using exact

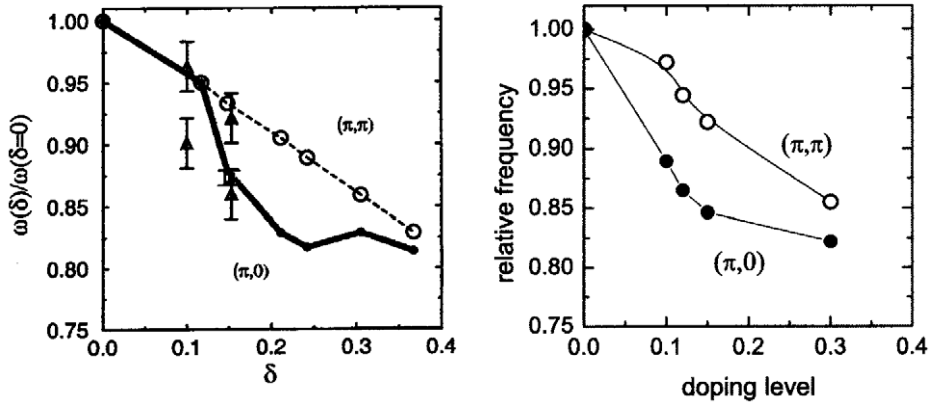

Figure 17. Relative softening of the half-breathing $(\pi, 0)$ and breathing phonons (π, π) as a function of doping δ. The left figure shows theoretical results of Horsch and Khaliullin [49] together with experimental results known at the time of the calculations and the right figure shows experimental results of Pintschovius *et al* [6] (after Pintschovius [6]).

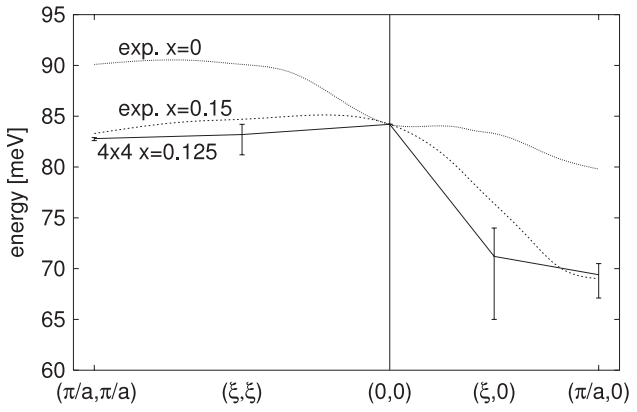

Figure 18. Phonon dispersion in the (1, 0) and (1, 1) directions. Experimental results (dotted line) for $x = 0$ and $x = 0.15$ are shown. Theoretical results (full curve) for $x = 0.125$ show the calculated softening from the experimental $x = 0$ results. The average over boundary conditions is shown and the bars show the spread due to different boundary conditions. There is a strong softening in the (1, 0) direction, while the softening in the (1, 1) direction is weaker at this doping (after Rösch and Gunnarsson [51]).

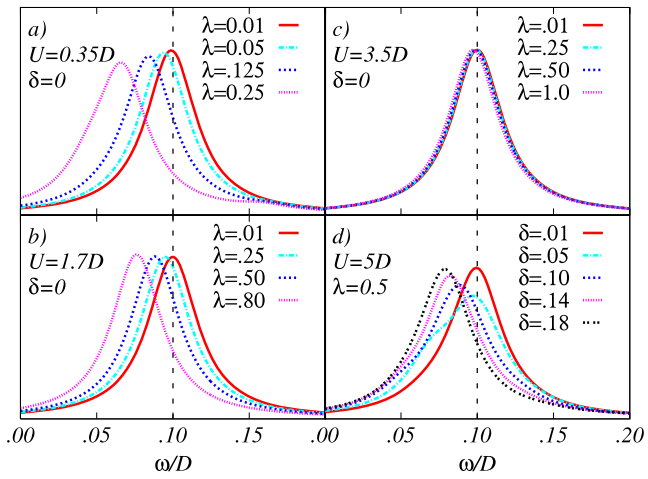

Figure 19. Phonon spectral function for different values of λ. The bare phonon frequency is $\omega_{\rm ph} = 0.1D$ and a Lorentzian broadening with the full width at half maximum of $0.04D$ has been introduced, where $D = W/2$ is half the band width. Parts (a)–(c) show how the phonon softening at half-filling is dramatically suppressed by U and (d) that the softening increases with doping δ (after Sangiovanni *et al* [71]).

diagonalization, including the phonons in the calculation, and the phonon spectral function was calculated. Their calculated dispersion for $\delta = 0.125$ is compared with experimental results in figure 18. The dotted curves show experimental results and the full curves the calculated softening for a 4×4 cluster. The bars show the spread of the results due to different (periodic, antiperiodic or mixed) boundary conditions. The figure illustrates that the softening is larger for the (1, 0) than the (1, 1) direction for this doping. The softening in the (1, 0) direction is large for $|\mathbf{q}| \gtrsim \pi/(2a)$. The softening essentially follows the coupling strength $\sim \sin^2(q_x a/2)$ but is larger at $q_x = \pi/(2a)$ than would be expected from this argument.

Sangiovanni *et al* [71] calculated the phonon softening within the AF–DMFT theory for the Holstein–Hubbard model. Figure 19(a) shows that there is a large softening for the undoped system if U is small. Figures 19(b) and (c) show how the softening is much smaller for larger values of U, although larger values of λ were used in figures 19(b) and (c). In particular, in figure 19(c) almost no softening is observed. Finally, figure 19(d) shows results for a doped system. As the doping is increased, the softening increases, although U is large. This illustrates the sum rule in equation (23) for phonons.

Falter *et al* [95, 96] have developed a model for the charge response of cuprates, including the ionic nature of the system. Based on this model they have calculated the softening of several phonons. In particular, they predicted the softening of the O_Z^Z phonon (see figure 1) [95, 96] before it was observed experimentally. For $La_{1.85}Sr_{0.15}CuO_4$ the softening of the O_Z^Z phonon is about 30% and its width is about 4 THz = 17 meV [5]. This large softening and width suggests a strong coupling to doped holes.

6.2. Phonon width

Khaliullin and Horsch [47] have calculated the width of the (half-) breathing phonon in the t–J model and found that it is very broad for $\mathbf{q} = (\pi, 0)$ due to the coupling to a low-lying collective mode in the density response function, while the $\mathbf{q} = (\pi, \pi)$ phonon is narrower for optimum doping. This is in good agreement with experiment.

It is interesting that LDA calculations [20] predict the frequency of the half-breathing phonon of $YBa_2Cu_3O_7$ quite accurately, while the theoretical width is an order of magnitude smaller than the width measured for $La_{2-x}Sr_xCuO_4$ [5]. Since the shift (real part) and width (imaginary part) are both determined by the phonon self-energy, and since the real and imaginary parts are related via the Kramers–Kronig relation, this is a surprising result. This was addressed [22] by projecting the three-band model onto a one-band model using either the Hartree–Fock (HF) approximation or by including many-body effects using the Zhang–Rice method [43] to obtain the t–J model. The HF approximation shows similarities to the LDA approach. As discussed in section 5.6.1, many-body effects enhance the EPI coupling constants in the derivation of a t–J model. On the other hand, based on a sum rule in section 5.1.1, many-body effects lead to a strongly doping dependent suppression of the EPI for the phonon self-energy. These two effects were shown to roughly cancel for $\delta \approx 0.15$ for the phonon softening [22]. Due to many-body effects, however, there are particularly many low-lying excitations which couple strongly to the half-breathing phonon and lead to a large width for this phonon [22, 46–49]. This effect is not present in the HF approximation [22].

7. Electron spectral function

7.1. Polaronic behavior in the undoped system

7.1.1. Quasiparticle weight in the absence of phonons. In section 4.3 we presented the arguments of Shen *et al* [7] that undoped cuprates show polarons. An essential part

of the argument was that the quasiparticle cannot be seen experimentally, because its weight Z is so strongly reduced by the interaction with the phonons. However, one could also imagine that coupling to spin fluctuations alone could have this effect, and there would then be no need to invoke phonons. We therefore first discuss whether or not Z is finite for the undoped t–J and Hubbard models.

Some approximate calculations for the t–J and Hubbard models gave $Z = 0$ for $\delta = 0$ [169, 170]. Similarly, DMFT calculations [79] for the paramagnetic state of the Hubbard model gave a very small Z for a small δ and a large U [163, 132], although later calculations including antiferromagnetic correlations using the AF–DMFT gave a substantial Z [171]. It is interesting that in the self-consistent Born approximation the carrier couples to magnons whose energies go to zero for $|\mathbf{q}| \to 0$. There is, however, no infrared singularity, since the coupling also goes to zero, and the quasiparticle weight converges to a finite number as the system size goes to infinity [156].

Exact diagonalization calculations for undoped t–J clusters with 16, 18, 20, 26 and 32 sites obtained finite values for Z, and there was no sign of Z going to zero with increasing cluster size [30, 172]. Brunner *et al* [173] studied a 24×24 t–J cluster using a loop algorithm and extrapolated the results to the thermodynamic limit. Mishchenko *et al* [174] calculated the Green's function $G_k(\tau)$ for imaginary times τ at $k = (\pi/2, \pi/2)$ for a 32×32 t–J cluster. By using a continuous-time worm algorithm [175] they could eliminate any systematic errors. From the τ dependence of $G_k(\tau)$ and from analytical continuation [176] they obtained Z. Both groups [173, 174] found values of Z similar to what had been obtained by exact diagonalization for small clusters. These results strongly suggest that Z stays finite for $\delta = 0$, and that therefore the lack of a visible quasiparticle in ARPES for undoped cuprates is due to the electron–phonon coupling.

7.1.2. Effects of phonons. In view of the results in the previous section, it is then natural to ask if the electron–phonon coupling is strong enough to give polaronic behavior. This was studied for La_2CuO_4 [23] within the t–J model together with a shell model [81] for describing the phonon eigenvectors. From the eigenvectors one can calculate the electrostatic potential acting on a Zhang–Rice singlet due to the excitation of a phonon, which provides an essential part of the coupling. In addition, the phonons modulate the Cu–O hopping integrals and the energy difference between the Cu and O levels in the three-band model used to derive the t–J model. This leads to an additional coupling mechanism. Defining the coupling as

$$\lambda = 2 \sum_{\mathbf{q}\nu} |g_{\mathbf{q}\nu}|^2 / (8t\omega_{\mathbf{q}\nu} N), \tag{32}$$

$\lambda = 1.2$ was obtained [23]. This is well above the values $\lambda_c = 0.4$ for the Holstein–t–J model [69] and $\lambda_c = 0.55$ for the Holstein–Hubbard model [71] giving small polarons.

We find that the dominating coupling for La_2CuO_4 is due to the (half-) breathing phonons, several apical oxygen phonons and some low-lying modes involving mainly La and Cu atoms. This is supported by inelastic neutron scattering experiments, showing a large broadening and softening under doping for the (half-) breathing and O_Z^Z apical oxygen phonons.

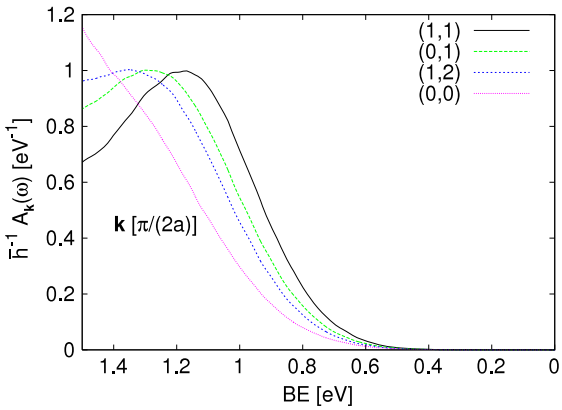

Figure 20. ARPES spectra for the undoped system at $T = 0$ for different $\mathbf{k}$ normalized to the height of the phonon side band and as a function of the binding energy (BE) (after Rösch and Gunnarsson [23]).

The resulting t–J model with phonons was solved using a method based on a statistical sampling of the phonons and exact diagonalization [23, 177, 164]. The results are shown in figure 20. The binding energy is measured in relation to the quasiparticle, which is too small to be seen. The peaks at about -1.1 to -1.3 eV are phonon side bands due to many unresolved phonon satellites. The width (0.5 eV) of the side band is close to the experimental result (0.48 eV) [23], and also the T-dependence is in agreement with experimental observations [23, 178]. The binding energy of the phonon side band is too large compared with experiment, which may indicate that the calculation overestimated the coupling strength. Reducing all coupling constants by a factor of 0.8 (giving $\lambda = 0.75$) gives the width 0.4 eV and the binding energy 0.6 eV, in reasonable agreement with the experimental results 0.48 and 0.5 eV, respectively. These results suggest that the EPI is sufficiently strong to give the polaronic behavior seen experimentally.

As discussed in section 4.3, the dispersion of the main peak in ARPES spectra of undoped cuprates can be well described by the dispersion of the quasiparticle in an extended t–J model with up to third nearest neighbor hopping [32]. However, this model cannot explain the large width of the peaks. Shen *et al* [7] therefore proposed that the peaks are actually not quasiparticles but phonon side bands. This then raises the question of why the phonon side bands should disperse like the quasiparticles in a model without phonons. Mishchenko and Nagaosa [69] performed diagrammatic Monte Carlo calculations for a t–J model with and without phonons. Their results are shown in figure 21. For $\lambda = 0.46$ there is a well developed phonon side band (filled circles) which is found to very closely follow the dispersion of the quasiparticle peak for $\lambda = 0$ (full line), strongly supporting the interpretation of Shen *et al* [7]. A simple explanation of the results of Mishchenko and Nagaosa [69] has been given [177]. As expected, the weak quasiparticle (filled squares) for $\lambda = 0.46$ shows almost no dispersion. For $\lambda = 0.4$ the phonon side band is less well developed.

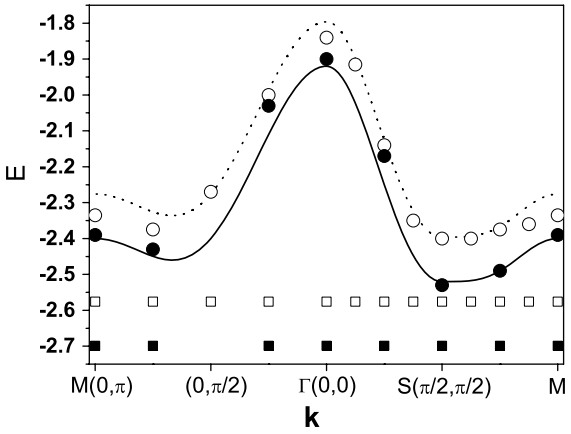

Figure 21. Dispersion of the phonon side band (filled circles) and the quasiparticle (filled squares) for $\lambda = 0.46$ as well as the dispersion of a broad peak (open circles) and the quasiparticle (open squares) for $\lambda = 0.4$. The two curves show the dispersion of a pure t–J model [179, 155] with the energy zeros defined appropriately for comparison with $\lambda = 0.46$ (full line) and $\lambda = 0.40$ (dotted line) (after Mishchenko and Nagaosa [69]).

7.2. Differences between phonons and spin fluctuations

The t–J model with one hole can be replaced by a model where the hole couples to magnons, treated as bosons [153–157]. In this approximation, phonons and spin fluctuations are treated on the same footing and can be directly compared. In particular, we can compare the couplings as defined by equation (32). The coupling to the magnons is then $\lambda_M = t/(2J) = 1.67$ for $J/t = 0.3$ while the coupling to phonons is only $\lambda = 1.2$ or 0.75 according to the estimates in section 7.1.2. It is then interesting to ask why spin fluctuations alone can not drive polaron formation.

Mishchenko and Nagaosa [69] and as well as Ciuchi *et al* [73, 159] pointed out that in a diagrammatic description polaron formation requires the inclusion of diagrams where lines describing phonon Green's functions cross. Liu and Manousakis [157] showed that for symmetry reasons whole classes of such diagrams are identically zero for coupling to magnons. This should be an essential reason why magnons alone cannot lead to polarons in the sense that the quasiparticle weight goes exponentially to zero as is the case for coupling to phonons. Alternatively, one can notice that polaron formation for Holstein phonons involves the excitation of many phonons on the same site as the hole. The magnons are due to flipping spins with $s = 1/2$, and locally it is only possible to flip such a spin once. This is in contrast to local phonons, which are true bosons and can be excited infinitely many times.

7.3. Kinks

Much of the interest in the EPI in the context of cuprates was triggered as Lanzara *et al* [8] emphasized the presence of kinks in the dispersion of the photoemission spectrum (see figure 5). There have been a large number of theoretical studies of this effect [180–185, 65, 59, 187–189]. An extensive theoretical study was performed by Sandvik *et al* [65], who solved the Eliashberg equations approximately, considering coupling to Holstein, breathing and buckling phonons as well as to the resonance peak seen in neutron scattering. The **q** dependence of the coupling for these modes is assumed to be rather different. The calculated spectra, however, did not show large qualitative differences. It was concluded that from the **q** dependence alone it might be hard to determine which mode causes the main coupling [65].

Devereaux *et al* [59] performed similar calculations, focusing on the coupling to breathing (at $\omega_{\mathrm{Br}} = 70$ meV) and B_{1g} buckling (at $\omega_{B_{1g}} = 36$ meV) phonons and comparing with experimental results for $Bi_2Sr_2Ca_{0.92}Y_{0.08}Cu_2O_{8+\delta}$. They argued that the B_{1g} phonon in particular couples to the antinodal point while the breathing phonon couples mainly to the nodal point. In the superconducting state, they found a structure in the antinodal direction at about $\omega_{B_{1g}} + \Delta = 71$ meV, where $\Delta = 35$ meV is the gap, while in the nodal direction they found a structure at about $\omega_{\mathrm{Br}} = 70$ meV. The effects of the c-axis O phonons on the kink have been studied by Meevasana *et al* [110, 168], as discussed in section 5.6.2.

Norman *et al* [111] noticed that the peak–dip–hump feature seen at the antinodal point below T_c could be explained by a coupling to the resonance peak, since this peak also only appears below T_c, has the right energy and would couple particularly strongly to the antinodal point. It was concluded that there may be a strong coupling to this resonance. This led to a substantial amount of work [180, 182–185, 187] describing a kink in terms of the coupling to spin fluctuations and to the resonance peak.

The kink is particularly pronounced in the antinodal direction in multilayer systems below T_c. The resonance peak is observed under these conditions, and it may therefore contribute to the kink. For symmetry reasons, the B_{1g} buckling phonon has a substantial coupling for multilayer systems [59]. The pile-up of density of states around the superconducting gap should enhance the contribution of the B_{1g} phonon to the kink for $T < T_c$ [59]. This makes it hard to determine the relative importance of the resonance peak and the B_{1g} phonon for the kink in the antinodal direction in multilayer systems.

Eschrig and Norman [183] observed that since the resonance peak is seen for bilayer systems in the odd channel it couples bonding (with respect to the two layers) to antibonding states. Since there is a large density of antibonding states close to the Fermi energy, the resonance peak should in particular influence the bonding state. They concluded [183] that the spectra of Bi2212 close to the antinodal point, interpreted in terms of antibonding and bonding states with peak–dip–hump structures [186], could be described if a sharp mode was introduced in the odd channel but not in the even channel. An interesting question is what happens if there is a sharp mode in both channels, as expected for phonons in the CuO_2 plane.

Heid *et al* [188] and Giustino *et al* [189] have calculated the magnitude of the kink using the electron–phonon coupling obtained from the LDA. The electron self-energy was then calculated assuming noninteracting electrons. They found that the calculated kink is almost an order of magnitude smaller than the experimentally observed kink, suggesting that the electron–phonon coupling is much too weak to explain the kink. It was found that the breathing phonons play a major

role for the kink [189]. Since the width of the half-breathing phonon is an order of magnitude too small in the LDA [20, 21], the LDA appears to greatly underestimate the coupling to this phonon and the relevance of the LDA calculation for the kink is unclear.

7.4. Isotope effect

There have been a number of theoretical studies of the isotope effect [190–195]. Andergassen *et al* [190] studied the phase diagram related to a quantum critical point (QCP) due to incommensurate charge ordering. Going beyond a mean-field theory by including fluctuations, they found that the QCP can be shifted by the isotope effect, leading to a general shift of the phase diagram. This shows up as a strong isotope effect in various properties [190]. Seibold and Grilli [192] argued that the correlation length for charge order fluctuations might have an isotope effect and found that this can lead to isotope effects in the PES spectra. Paci *et al* [191] studied the Holstein model and demonstrated a strong isotope effect in, e.g., the effective mass when the EPI was strong enough to put the system close to (small) polaron formation. In a study of the Holstein–Hubbard model, Paci *et al* [195] found that the competition between the Coulomb and electron–phonon interactions strongly influences the isotope effect. Mishchenko and Nagaosa [194] studied the undoped Holstein–t–J model using a diagrammatic Monte Carlo method. They found that the isotope effect can be large under certain circumstances.

8. Superconductivity

Honerkamp *et al* [167, 196] have studied the effects of phonons on the superconductivity transition using a weak coupling functional renormalization group method. They studied Holstein, breathing, A_{1g} and B_{1g} out-of-plane oxygen buckling modes. They found that the Holstein and A_{1g} phonons are unfavorable for d-wave superconductivity. These phonons add an on-site interaction, which reduces the Coulomb repulsion. In the weak coupling limit studied by Honerkamp *et al* [167, 196], this was found to be unfavorable for d-wave superconductivity. Of the phonons studied, only the B_{1g} phonon, which gives no on-site attraction for $\mathbf{q} = 0$, was found to be favorable for d-wave superconductivity.

Macridin *et al* [166, 197] performed DCA calculations for Hubbard model with coupling to Holstein, breathing and out-of-plane oxygen buckling phonons for a 2×2 cluster. The calculations neglected the EPI on the hopping integrals and thereby the $\mathbf{k}$ dependence of the coupling. The results for the transition temperature T_c are shown in figure 22. The figure shows how T_c drops with λ for all the phonon couplings considered. It was actually found that all phonons considered enhance the pairing, and it was speculated that this is due to an enhancement of the AF susceptibility [197]. The EPI, however, reduces the quasiparticle strength Z, and it was concluded that this is more important than the increase of the pairing, leading to a reduction of T_c [197]. It would be interesting to also study the effects of coupling to hopping integrals for the buckling modes and the effects for a larger U.

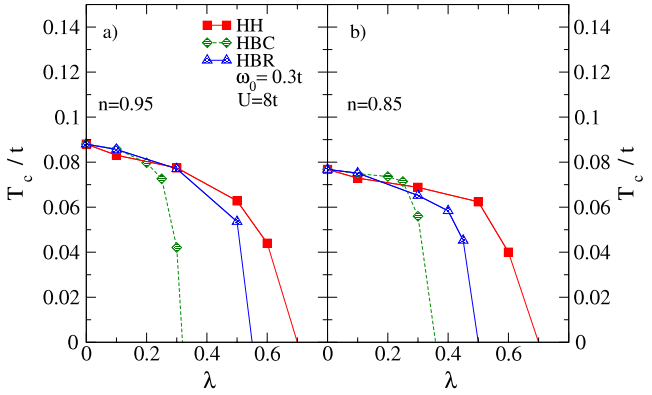

Figure 22. T_c versus λ for a Hubbard model with Holstein (HH), buckling (HBC) or breathing (HBR) phonons at (a) 5% and (b) 15% doping for $\omega_{ph} = 0.3t$ and $U = 8t$ (after Macridin *et al* [197]).

9. Summary

We have reviewed evidence that the electron–phonon interaction (EPI) can substantially influence various properties of the high-T_c cuprates. Some of the evidence is indirect and it can then be hard to determine which phonon modes are involved or to distinguish between phonons and other boson-like excitations, such as the resonance peak. It is therefore of particular interest that inelastic neutron scattering shows that certain phonon modes are appreciably broadened and shifted when the system is doped. This is strong evidence that these modes have a substantial EPI. In particular, such effects have been found for apical oxygen phonons and the (half-) breathing oxygen bond-stretching phonons. Theoretical many-body calculations indeed find substantial couplings for these phonons. For multilayer systems similar effects are also seen for other phonons, in particular the B_{1g} phonon. We have discussed theoretical treatments of phonon softening and broadening and illustrated that the experimental behavior can be described theoretically.

Much of the interest in the EPI was triggered by the observation of kinks in the dispersion seen in photoemission, which can be interpreted in terms of coupling to phonons. It remains controversial, however, how much phonons and the resonance peak or other spin excitations contribute to these kinks. Theoretical treatments of the kink have been shown.

There is strong evidence in favor of (small) polaron formation in undoped cuprates. While this polaron formation is helped by the antiferromagnetic correlations, we have argued that antiferromagnetic fluctuations alone could not lead to small polarons. This suggests a substantial EPI for the undoped cuprates. The EPI for $LaCuO_4$ has been calculated, obtaining substantial coupling to apical and breathing phonons, and it was shown that the experimental line shape of the photoemission spectra can be understood rather well. As the system is doped, the polarons disappear. Photoemission spectra, however, still show substantial weight in the energy range where the polaron related phonon side band was observed, suggesting that the EPI is substantial also in the doped systems.

An important feature of the cuprates is the great importance of the Coulomb repulsion. We have therefore treated the interplay between Coulomb and electron–phonon interactions extensively. Using sum rules, we showed that for weakly doped cuprates the Coulomb repulsion strongly suppresses the phonon self-energy, while there is no corresponding strong suppression of the electron self-energy. For polaron formation as seen in photoemission (described by the electron self-energy), antiferromagnetic correlations, resulting from the Coulomb repulsion, greatly help the EPI. Nevertheless, due to other effects of the Coulomb interaction, there is a moderate suppression of polaron formation, at least in the antiferromagnetic DMFT.

The EPI is usually discussed for some model with EPI, assuming that the electron–phonon coupling constants are fixed. We find, however, that when deriving, for instance, Holstein–t–J or Holstein–Hubbard models the coupling constants may be substantially enhanced by many-body effects. This is, for instance, the case for the (half-) breathing phonons.

References

[1] Kastner M A, Birgeneau R J, Shirane G and Endoh Y 1998 *Rev. Mod. Phys.* **70** 897
[2] Timusk T and Statt B 1999 *Rep. Prog. Phys.* **62** 61
[3] Varma C M, Littlewood P B and Schmitt-Rink S 1989 *Phys. Rev. Lett.* **63** 1996
[4] Bednorz J G and Müller K A 1986 *Z. Phys.* B **64** 189
[5] Pintschovius L and Reichardt W 1998 Neutron Scattering in Layered Copper-Oxide Superconductors, *Physics and Chemistry of Materials with Low-Dimensional Structures* vol 20 , ed A Furrer (Dordrecht: Kluwer–Academic) p 165
[6] Pintschovius L 2005 *Phys. Status Solidi* b **242** 30
[7] Shen K M *et al* 2004 *Phys. Rev. Lett.* **93** 267002
[8] Lanzara A *et al* 2001 *Nature* **412** 510
[9] Franck J P 1994 Experimental Studies of the isotope effect in high temperature superconductors *Physical Properties of High Temperature Superconductors IV* ed D M Ginsberg (Singapore: World Scientific) p 189
[10] Lee J *et al* 2006 *Nature* **442** 546
[11] Pilgram S, Rice T M and Sigrist M 2006 *Phys. Rev. Lett.* **97** 117003
[12] Kohn W and Sham L J 1965 *Phys. Rev.* **140** A1133
[13] Hohenberg P and Kohn W 1964 *Phys. Rev.* **136** B864
[14] Savrasov S Y, Savrasov D Y and Andersen O K 1994 *Phys. Rev. Lett.* **72** 372
[15] Savrasov S Y and Savrasov D Y 1996 *Phys. Rev.* B **54** 16487
[16] Marques M A, Lüders M, Lathiotakis N N, Profeta G, Floris A, Fast L, Continenza A, Gross E K and Massidda S 2005 *Phys. Rev.* B **72** 024546
[17] Lüders M, Marques M A, Lathiotakis N N, Floris A, Profeta G, Fast L, Continenza A, Massidda S and Gross E K 2005 *Phys. Rev.* B **72** 024545
[18] Pickett W E 1989 *Rev. Mod. Phys.* **61** 433
[19] Savrasov S Y and Andersen O K 1996 *Phys. Rev. Lett.* **77** 4430
[20] Bohnen K-P, Heid R and Krauss M 2003 *Europhys. Lett.* **64** 104 and private communication
[21] Pintschovius L and Braden M 1999 *Phys. Rev.* B **60** R15039
[22] Rösch O and Gunnarsson O 2004 *Phys. Rev.* B **70** 224518
[23] Rösch O, Gunnarsson O, Zhou X J, Yoshida T, Sasagawa T, Fujimori A, Hussain Z, Shen Z-X and Uchida S 2005 *Phys. Rev. Lett.* **95** 227002
[24] Alexandrov A S and Mott N 1995 *Polarons and Bipolarons* (Singapore: World Scientific)
[25] Lupi S, Maselli P, Capizzi M, Calvani P, Giura P and Roy P 1999 *Phys. Rev. Lett.* **83** 4852
[26] Calvani P 2001 *Optical Properties of Polarons* (Bologna: Editrice Compositori)
[27] Tempere J and Devreese J T 2001 *Phys. Rev.* B **64** 104504
[28] Alexandrov A S 2003 *Theory of Superconductivity: From Weak to Strong Coupling* (*Series in Condensed Matter Physics*) (Bristol: Institute of Physics)
[29] Devreese J T 2007 *J. Phys.: Condens. Matter* **19** 255201
[30] Dagotto E 1994 *Rev. Mod. Phys.* **66** 763
[31] Egami T and BillingeS J L 1996 lattice effects in high-T_c superconductors *Physical Properties of High Temperature Superconductors* V ed D M Ginsberg (Singapore: World Scientific) p 189
[32] Tohyama T and Maekawa S 2000 *Supercond. Sci. Technol.* **13** R17
[33] Kulic M L 2000 *Phys. Rep.* **338** 1
[34] Kivelson S A, Bindloss I P, Fradkin E, Oganesyan V, Tranquada J M, Kapitulnik A and Howald C 2003 *Rev. Mod. Phys.* **75** 1201
[35] Norman M R and Pepin C 2003 *Rep. Prog. Phys.* **66** 1547
[36] Fink J, Borisenko S, Kordyuk A, Koitzsch A, Geck J, Zabolotnyy V, Knupfer M, Büchner B and Berger H 2007 *Lect. Notes Phys.* **715** 295
[37] Norman M R, Pines D and Kallin C 2005 *Adv. Phys.* **54** 715
[38] Lee P A, Nagaosa N and Wen X-G 2006 *Rev. Mod. Phys.* **78** 17
[39] Zhou X J, Cuk T, Devereaux T, Nagaosa N and Shen Z-X 2006 *Preprint* cond-mat/0604284
[40] Yoshida T, Zhou X J, Lu D H, Komiya S, Ando Y, Eisaki H, Kakeshita T, Uchida S, Hussain Z, Shen Z-X and Fujimori A 2007 *J. Phys.: Condens. Matter* **19** 125209
[41] Egami T 2006 Polarons in complex oxides: CMR manganites and HTSC cuprates *Polarons in Bulk Materials and Systems with Reduced Dimensionality* (*Proc. Int. School of Physics 'Enrico Fermi' Course CLXI*) ed G Iadonisi, G De Filippis and J Ranninger (Amsterdam: IOS press) p 101
[42] Emery V J 1987 *Phys. Rev. Lett.* **58** 2794
[43] Zhang F C and Rice T M 1988 *Phys. Rev.* B **37** 3759
[44] Auerbach A 1994 *Interacting Electrons and Quantum Magnetism* (Berlin: Springer)
[45] von Szczepanski K J and Becker K W 1992 *Z. Phys.* B **89** 327
[46] Khaliullin G and Horsch P 1996 *Phys. Rev.* B **54** R9600
[47] Khaliullin G and Horsch P 1997 *Physica* C **282–287** 1751
[48] Horsch P, Khaliullin G and Oudovenko V 2000 *Physica* C **341–348** 117
[49] Horsch P and Khaliullin G 2005 *Physica* B **359–361** 620
[50] Ishihara S and Nagaosa N 2004 *Phys. Rev.* B **69** 144520
[51] Rösch O and Gunnarsson O 2004 *Phys. Rev. Lett.* **92** 146403
[52] Bulut N and Scalapino D J 1996 *Phys. Rev.* B **54** 14971
[53] Friedl B, Thomsen C and Cardona M 1990 *Phys. Rev. Lett.* **65** 915
[54] Pyka N, Reichardt W, Pintschovius L, Engel G, Rossat-Mignod J and Henry J Y 1993 *Phys. Rev. Lett.* **70** 1457
[55] Reznik D, Keimer B, Dogan F and Aksay I A 1995 *Phys. Rev. Lett.* **75** 2396
[56] Devereaux T P, Virosztek A and Zawadowski A 1995 *Phys. Rev.* B **51** 505
[57] Opel M, Hackl R, Devereaux T P, Virosztek A, Zawadowski A, Erb A, Walker E, Berger H and Forro L 1999 *Phys. Rev.* B **60** 9836
[58] Devereaux T P, Virosztek A and Zawadowski A 1999 *Phys. Rev.* B **59** 14618
[59] Devereaux T P, Cuk T, Shen Z-X and Nagaosa N 2004 *Phys. Rev. Lett.* **93** 117004
[60] Rashba E and Sherman E 1988 *JETP Lett.* **47** 482

[61] Jepsen O, Andersen O K, Dasgupta I and Savrasov S 1998 *J. Phys. Chem. Solids* **59** 1718
[62] Mahan G D 1981 *Many-Particle Physics* (New York: Plenum)
[63] Engelsberg S and Schrieffer J R 1963 *Phys. Rev.* **131** 993
[64] Scalapino D J 1969 The electron-phonon interaction and strong-coupling superconductors *Superconductivity* ed R D Parks (New York: Dekker) p 449
[65] Sandvik A W, Scalapino D J and Bickers N E 2004 *Phys. Rev.* B **69** 094523
[66] Allen P B 1972 *Phys. Rev.* B **6** 2577
[67] Allen P B 1974 *Solid State Commun.* **14** 937
[68] Ramsak A, Horsch P and Fulde P 1992 *Phys. Rev.* B **46** 14305
[69] Mishchenko A S and Nagaosa N 2004 *Phys. Rev. Lett.* **93** 036402
[70] Fehske H, Loos J and Wellein G 2000 *Phys. Rev.* B **61** 8016
[71] Sangiovanni G, Gunnarsson O, Koch E, Castellani C and Capone M 2006 *Phys. Rev. Lett.* **97** 046404
[72] Millis A J, Mueller R and Shraiman B I 1996 *Phys. Rev.* B **54** 5389
[73] Ciuchi S, de Pasquale F, Fratini S and Feinberg D 1997 *Phys. Rev.* B **56** 4494
[74] Benedetti P and Zeyher R 1998 *Phys. Rev.* B **58** 14320
[75] Meyer D, Hewson A C and Bulla R 2002 *Phys. Rev. Lett.* **89** 196401
[76] Han J E, Gunnarsson O and Crespi V H 2003 *Phys. Rev. Lett.* **90** 167006
[77] Capone M and Ciuchi S 2003 *Phys. Rev. Lett.* **91** 186405
[78] Capone M, Carta P and Ciuchi S 2006 *Phys. Rev.* B **74** 045106
[79] Georges A, Kotliar G, Krauth W and Rozenberg M J 1996 *Rev. Mod. Phys.* **68** 13
[80] Capone M, Stephan W and Grilli M 1997 *Phys. Rev.* B **56** 4484
[81] Chaplot S L, Reichardt W, Pintschovius L and Pyka N 1995 *Phys. Rev.* B **52** 7230
[82] Pintschovius L, Reznik D and Yamada K 2006 *Phys. Rev.* B **74** 174514
[83] Pintschovius L, Pyka N, Reichardt W, Rumiantsev A Y, Mitrofanov N L, Ivanov A S, Collin G and Bourges P 1991 *Physica* C **185–189** 156
[84] Reichardt W 1996 *J. Low Temp. Phys.* **105** 807
[85] Pintschovius L and Braden M 1996 *J. Low Temp. Phys.* **105** 813
[86] McQueeney R J, Petrov Y, Egami T, Yethiraj M, Shirane G and Endoh Y 1999 *Phys. Rev. Lett.* **82** 628
[87] McQueeney R J, Sarrao J L, Pagliuso P G, Stephens P W and Osborn R 2001 *Phys. Rev. Lett.* **87** 077001
[88] Pintschovius L, Reichardt W, Kläser M, Wolf T and v Löhneysen H 2002 *Phys. Rev. Lett.* **89** 037001
[89] Chung J-H *et al* 2003 *Phys. Rev.* B **67** 014517
[90] Tranquada J M, Nakajima K, Braden M, Pintschovius L and McQueeney R J 2002 *Phys. Rev. Lett.* **88** 075505
[91] Reichardt W and Braden M 1999 *Physica* B **263/264** 416
[92] Braden M, Reichardt W, Shiryaev S and Barilo S N 2002 *Physica* C **378–381** 89
[93] Mattheiss L F 1987 *Phys. Rev. Lett.* **58** 1028
[94] Reznik D, Pintschovius L, Ito M, Iikubo S, Sato M, Goka H, Fujita M, Yamada K, Gu G D and Tranquada J M 2006 *Nature* **440** 1170
[95] Falter C and Klenner M 1994 *Phys. Rev.* B **50** 9426
[96] Falter C, Klenner M and Hoffmann G A 1995 *Phys. Rev.* B **52** 3702
[97] Macfarlane R M, Rosen H and Seki H 1987 *Solid State Commun.* **63** 831
[98] Cooper S L, Klein M V, Pazol B G, Rice J P and Ginsberg D M 1988 *Phys. Rev.* B **37** 5920
[99] Thomsen C, Cardona M, Gegenheimer B, Liu R and Simon A 1988 *Phys. Rev.* B **37** 9860
[100] Thomsen C, Cardona M, Friedl B, Rodriguez C O, Mazin I I and Andersen O K 1990 *Solid State Commun.* **75** 219
[101] Harashina H, Kodama K, Shamoto S, Sato M, Kakurai K and Nishi M 1996 *Physica* C **263** 257
[102] Valla T, Fedorov A V, Johnson P D, Wells B O, Hulbert S L, Li Q, Gu G D and Koshizuka N 1999 *Science* **285** 2110
[103] Kaminski A *et al* 2000 *Phys. Rev. Lett.* **84** 1788
[104] Bogdanov P V *et al* 2000 *Phys. Rev. Lett.* **85** 2581
[105] Kaminski A, Randeria M, Campuzano J C, Norman M R, Fretwell H, Mesot J, Sato T, Takahashi T and Kadowaki K 2001 *Phys. Rev. Lett.* **86** 1070
[106] Johnson P D *et al* 2001 *Phys. Rev. Lett.* **87** 177007
[107] Gromko A D, Fedorov A V, Chuang Y-D, Koralek J D, Aiura Y, Yamaguchi Y, Oka K, Ando Y and Dessau D S 2003 *Phys. Rev.* B **68** 174520
[108] Sato T *et al* 2003 *Phys. Rev. Lett.* **91** 157003
[109] Zhou X J *et al* 2005 *Phys. Rev. Lett.* **95** 117001
[110] Meevasana W *et al* 2006 *Phys. Rev. Lett.* **96** 157003
[111] Norman M R, Ding H, Campuzano J C, Takeuchi T, Randeria M, Yokoya T, Takahashi T, Mochiku T and Kadowaki K 1997 *Phys. Rev. Lett.* **79** 3506
[112] Kim T K, Kordyuk A A, Borisenko S V, Koitzsch A, Knupfer M, Berger H and Fink J 2003 *Phys. Rev. Lett.* **91** 167002
[113] Cuk T *et al* 2004 *Phys. Rev. Lett.* **93** 117003
[114] Norman M R and Ding H 1998 *Phys. Rev.* B **57** R11089
[115] Rossat-Mignod J, Regnault L P, Vettier C, Bourges P, Burlet P, Bossy J, Henry J Y and Lapertot G 1991 *Physica* C **185–189** 86
[116] Mook H A, Yethiraj M, Aeppli G, Mason T E and Armstrong T 1993 *Phys. Rev. Lett.* **70** 3490
[117] Fong H F, Keimer B, Anderson P W, Reznik D, Dogan F and Aksay I A 1995 *Phys. Rev. Lett.* **75** 316
[118] Fong H F, Bourges P, Sidis Y, Regnault L P, Ivanov A, Gu G D, Koshizuka N and Keimer B 1999 *Nature* **398** 588
[119] Vignolle B, Hayden S M, McMorrow D F, Ronnow H M, Lake B, Frost C D and Perring T G 2007 *Nat. Phys.* **3** 163
[120] Shen K M *et al* 2007 *Phys. Rev.* B **75** 075115
[121] Yoshida T *et al* 2003 *Phys. Rev. Lett.* **91** 027001
[122] Yoshida T *et al* 2006 *Phys. Rev.* B **74** 224510
[123] Khasanov R *et al* 2004 *Phys. Rev. Lett.* **92** 057602
[124] Gweon G-H, Sasagawa T, Zhou S Y, Graf J, Takagi H, Lee D-H and Lanzara A 2004 *Nature* **430** 187
[125] Douglas J F *et al* 2007 *Nature* **446** E5
[126] Gweon G-H, Sasagawa T, Takagi H, Lee D-H and Lanzara A 2007 *Preprint* cond-mat/07081027
[127] Iwasawa H and Douglas J F *et al* 2007 to be published
[128] Hoffman J E, McElroy K, Lee D-H, Lang K M, Eisaki H, Uchida S and Davis J C 2002 *Science* **297** 1148
[129] McElroy K, Simmonds R W, Hoffman J E, Lee D-H, Orenstein J, Eisaki H, Uchida S and Davis J C 2003 *Nature* **422** 592
[130] Hanaguri T, Lupien C, Kohsaka Y, Lee D-H, Azuma M, Takano M, Takagi H and Davis J C 2004 *Nature* **430** 1001
[131] Kim J H and Tesanovic Z 1993 *Phys. Rev. Lett.* **71** 4218
[132] Sangiovanni G, Capone M and Castellani C 2006 *Phys. Rev.* B **73** 165123
[133] Rösch O and Gunnarsson O 2004 *Phys. Rev. Lett.* **93** 237001
[134] Rösch O, Sangiovanni G and Gunnarsson O 2007 *Phys. Rev.* B **75** 035119
[135] Kulic M L and Zeyher R 1994 *Phys. Rev.* B **49** 4395
[136] Grilli M and Castellani C 1994 *Phys. Rev.* B **50** 16880
[137] Zeyher R and Kulic M L 1996 *Phys. Rev.* B **53** 2850
[138] Huang Z B, Hanke W, Arrigoni E and Scalapino D J 2003 *Phys. Rev.* B **68** 220507(R)
[139] Cappelluti E, Cerruti B L and Pietronero L 2004 *Phys. Rev.* B **69** 161101(R)
[140] Koch E and Zeyher R 2004 *Phys. Rev.* B **70** 094510

[141] Kulic M L and Dolgov O V 2005 *Phys. Rev.* B **71** 092505
[142] Blankenbecler R, Scalapino D J and Sugar R L 1981 *Phys. Rev.* D **24** 2278
[143] Ranninger J and Thibblin U 1992 *Phys. Rev.* B **45** 7730
[144] Zhong J and Schüttler H-B 1992 *Phys. Rev. Lett.* **69** 1600
[145] Lorenzana J and Dobry A 1994 *Phys. Rev.* B **50** 16094
[146] Röder H, Fehske h and Silver R N 1994 *Europhys. Lett.* **28** 257
[147] Fehske H, Röder H, Wellein G and Mistriotis A 1995 *Phys. Rev.* B **51** 16582
[148] Wellein G, Röder H and Fehske H 1996 *Phys. Rev.* B **53** 9666
[149] Sakai T, Poilblanc D and Scalapino D J 1997 *Phys. Rev.* B **55** 8445
[150] Bäuml B, Wellein G and Fehske H 1998 *Phys. Rev.* B **58** 3663
[151] Fehske H, Wellein G, Hager G, Weiße A and Bishop A R 2004 *Phys. Rev.* B **69** 165115
[152] Prelovsek P, Zeyher R and Horsch P 2006 *Phys. Rev. Lett.* **96** 086402
[153] Schmitt-Rink S, Varma C M and Ruckenstein A E 1988 *Phys. Rev. Lett.* **60** 2793
[154] Kane C L, Lee P A and Read N 1989 *Phys. Rev.* B **39** 6880
[155] Marsiglio F, Ruckenstein A E, Schmitt-Rink S and Varma C M 1991 *Phys. Rev.* B **43** 10882
[156] Martinez G and Horsch P 1991 *Phys. Rev.* B **44** 317
[157] Liu Z and Manousakis E 1992 *Phys. Rev.* B **45** 2425
[158] Gunnarsson O and Rösch O 2006 *Phys. Rev.* B **73** 174521
[159] Cappelluti E and Ciuchi S 2002 *Phys. Rev.* B **66** 165102
[160] Cappelluti E, Ciuchi S and Fratini S 2007 *Phys. Rev.* B **76** 125111
[161] Toschi A and Capone M 2007 *Preprint* 0708.3475
[162] Capone M, Sangiovanni G, Castellani C, Di Castro C and Grilli M 2004 *Phys. Rev. Lett.* **92** 106401
[163] Sangiovanni G, Capone M, Castellani C and Grilli M 2005 *Phys. Rev. Lett.* **94** 026401
[164] Schönhammer K and Gunnarsson O 1984 *Phys. Rev.* B **30** 3141
[165] Gunnarsson O and Schönhammer K 1983 *Phys. Rev.* B **28** 4315
[166] Macridin A, Moritz B, Jarrell M and Maier T 2006 *Phys. Rev. Lett.* **97** 056402
[167] Fu H C, Honerkamp C and Lee D-H 2006 *Europhys. Lett.* **75** 146
[168] Meevasana W, Devereaux T P, Nagaosa N, Shen Z-X and Zaanen J 2006 *Phys. Rev.* B **74** 174524
[169] Sheng D N, Chen Y C and Weng Z Y 1996 *Phys. Rev. Lett.* **77** 5102
[170] Paramekanti A, Randeria M and Trivedi N 2001 *Phys. Rev. Lett.* **87** 217002
[171] Sangiovanni G *et al* 2006 *Phys. Rev.* B **73** 205121
[172] Leung P W and Gooding R J 1995 *Phys. Rev.* **52** R15711
[173] Brunner M, Assaad F F and Muramatsu A 2000 *Phys. Rev.* B **62** 15480
[174] Mishchenko A S, Prokof'ev N V and Svistunov B V 2001 *Phys. Rev.* B **64** 033101
[175] Prokof'ev N V, Svistunov B V and Tupitsyn I S 1998 *Sov. Phys.—JETP* **87** 310
[176] Mishchenko A S, Prokof'ev N V, Sakamoto A and Svistunov B V 2000 *Phys. Rev.* B **62** 6317
[177] Rösch O and Gunnarsson O 2005 *Eur. Phys. J.* B **43** 11
[178] Cataudella V, de Filippis G, Mishchenko A and Sand Nagaosa N 2007 *Preprint* cond-mat/07073076
[179] Horsch P, Stephan W H, Szczepanski K v, Ziegler M and von der Linden W 1989 *Physica* C **162–164** 783
[180] Eschrig M and Norman M R 2000 *Phys. Rev. Lett.* **85** 3261
[181] Zeyher R and Greco A 2001 *Phys. Rev.* B **64** 140510(R)
[182] Manske D, Eremin I and Bennemann K H 2001 *Phys. Rev. Lett.* **87** 177005
[183] Eschrig M and Norman M R 2002 *Phys. Rev. Lett.* **89** 277005
[184] Manske D, Eremin I and Bennemann K H 2003 *Phys. Rev.* B **67** 134520
[185] Chubukov A V and Norman M R 2004 *Phys. Rev.* B **70** 174505
[186] Feng D L *et al* 2001 *Phys. Rev. Lett.* **86** 5550
[187] Manske D 2004 *Theory of Unconventional Superconductors: Cooper-Pairing Mediated by Spin Excitations* (*Springer Tracts in Modern Physics* vol 202) (Heidelberg: Springer)
[188] Heid R, Bohnen K-P, Zeyher R and Manske D 2007 *Preprint* 0707.4429
[189] Giustino F, Cohen M L and Louie S G 2007 *Preprint* 0710.2146
[190] Andergassen S, Caprara S, Di Castro C and Grilli M 2001 *Phys. Rev. Lett.* **87** 056401
[191] Paci P, Capone M, Cappelluti E, Ciuchi S, Grimaldi C and Pietronero L 2005 *Phys. Rev. Lett.* **94** 036406
[192] Seibold G and Grilli M 2005 *Phys. Rev.* B **72** 104519
[193] Fratini S and Ciuchi S 2005 *Phys. Rev.* B **72** 235107
[194] Mishchenko A S and Nagaosa N 2006 *Phys. Rev.* B **73** 092502
[195] Paci P, Capone M, Cappelluti E, Ciuchi S and Grimaldi C 2006 *Phys. Rev.* B **74** 205108
[196] Honerkamp C, Fu H C and Lee D-H 2007 *Phys. Rev.* B **75** 014503
[197] Macridin A, Moritz B, Jarrell M and Maier T 2006 *Preprint* cond-mat/0611067